Palaeobiodiversity and Palaeoenvironments (2022) 102:331–350
https://doi.org/10.1007/s12549-021-00511-1

SENCKENBERG

ORIGINAL PAPER

The Permian–Triassic boundary section at Baghuk Mountain, Central Iran: carbonate microfacies and depositional environment

Franziska Heuer[1] · Lucyna Leda[1] · Hemen Moradi-Salimi[1,2] · Jana Gliwa[1,3] · Vachik Hairapetian[4] · Dieter Korn[1]

Received: 22 March 2021 / Revised: 22 July 2021 / Accepted: 4 August 2021 / Published online: 3 November 2021

Abstract

Sections at Baghuk Mountain, 45 km NNW of Abadeh (Central Iran), have excellent exposures of fossiliferous marine Late Permian to Early Triassic sedimentary successions. Detailed bed-by-bed sampling enables the analysis of microfacies changes of three successive rock units across the Permian–Triassic boundary. The Late Permian Hambast Formation is mainly the result of biogenic carbonate production. Its carbonate microfacies is dominated by biogen-rich and bioturbated nodular limestones, indicating a well-oxygenated aphotic to dysphotic environment. The biogen-dominated carbonate factory in the Permian ceased simultaneously with the main mass extinction pulse, which is marked by a sharp contact between the Hambast-Formation and the overlaying Baghuk Member (= 'Boundary Clay'). The clay and silt deposits of the Baghuk Member with some carbonate beds show only a few signs of bioturbation or relics of benthic communities. The Early Triassic *Claraia* Beds are characterised by a partly microbially induced carbonate production, which is indicated by frequent microbialite structures. The depositional environment does not provide evidence of large amplitude changes of sea level or subaerial exposure during the Permian–Triassic boundary interval. The deposition of the Baghuk Mountain sediments took place in a deep shelf environment, most of the time below the storm wave base.

Keywords Permian–Triassic boundary · Central Iran · Carbonate microfacies · Microbialites · Sponges

✉ Dieter Korn
dieter.korn@mfn.berlin

Franziska Heuer
franziska.heuer@gmx.de

Lucyna Leda
lucyna.skorpion3@wp.pl

Hemen Moradi-Salimi
hemen.ku@gmail.com

Jana Gliwa
jana.gliwa@gmail.com

Vachik Hairapetian
vhairap@gmail.com

[1] Museum Für Naturkunde, Leibniz Institute for Research On Evolution and Biodiversity, Invalidenstraße 43, 10115 Berlin, Germany

[2] Geology Department, Faculty of Science, University of Isfahan, Isfahan, Iran

[3] Eurasia Department and Beijing Branch Office, German Archaeological Institute, Berlin, Germany

[4] Department of Geology, Islamic Azad University, PO Box 81595-158, Isfahan (Khorasgan) BranchIsfahan, Iran

Introduction

The catastrophic Late Permian mass extinction resulted in dramatic changes in biodiversity (e.g. Raup and Sepkoski 1982, 1984; Erwin 1993, 1994; Stanley and Yang 1994; Erwin et al. 2002) paralleled by shifts in chemistry in the Tethys Ocean (e.g. Baud et al. 1989; Heydari et al. 2000; Korte et al. 2004a, b; Schobben et al. 2015, 2017). While there is agreement on a significant increase in seawater temperatures (Joachimski et al. 2012, 2020; Sun et al. 2012; Chen et al. 2013, 2020; Schobben et al. 2014), there is a vigorous debate, whether the Permian–Triassic (P-Tr) transition was associated with significant sea-level changes and global anoxia (e.g. Wignall and Hallam 1992; Knoll et al. 1996; Wignall and Twitchett 1996; Hallam and Wignall 1999; Berner 2006; Bond and Wignall 2010; Zhang et al. 2018; Schobben et al. 2020). Previous studies suggested that the formation of microbial communities, which occur particularly in Early Triassic successions, is either a consequence of global oceanic alkalinity changes and changes in carbonate saturation or the response of the widespread extinction of metazoans and the resulting replacement of

skeletal carbonates (e.g. Baud et al. 1997, 2007; Kershaw et al. 1999, 2002, 2007, 2011, 2012; Mata and Bottjer 2012; Forel et al. 2013; Chen et al. 2014; Fang et al. 2017).

In the area south-east of Abadeh, Permian–Triassic boundary sections were described for the first time 50 years ago (Taraz 1969, 1971, 1973). After these pioneering studies, further monographic articles played an important role in contributing to knowledge of the most severe extinction event in the Phanerozoic (Bando 1979, 1981; Taraz et al. 1981). The sections in the area around Kuh-e-Hambast (=Hambast Range) were intensively investigated to explain in detail external influences like global warming and redox conditions in the ocean. Descriptions of microfacies (e.g. Baud et al. 1997), investigations of sedimentary successions paralleled by mineralogical and geochemical studies (e.g. Heydari et al. 2000) and isotope $\delta^{18}O$ studies on whole rock carbonates (e.g. Korte et al. 2004a, b) were carried out at the Hambast section.

However, studies related to the macrofossils of these sections had only been conducted for a few groups of invertebrates, for example ammonoids (Bando 1979, 1981; Taraz et al. 1981; Zakharov et al. 2010). Although various groups of fossils are present in a number of horizons, no detailed analysis of the decline of Late Permian biota has been achieved. The sections of the Hambast Range in the Abadeh region consist almost exclusively of carbonates with thin shale deposits deposited at a deeper shelf (Kozur 2007).

Sections at Baghuk Mountain (Fig. 1), which are located 45 km north-west of Abadeh (Central Iran), represent uninterrupted sedimentary successions across the P-Tr transition (Leda et al. 2014; Leda 2020). Therefore, studies in this area are of great value for understanding the effects and possible causes of environmental changes during the transition from the Palaeozoic to the Mesozoic. These sections provide the opportunity to study the Wuchiapingian to Dienerian sedimentary succession in terms of lithology, carbonate microfacies, fossil content (particularly ammonoids, bivalves, brachiopods, conodonts, ostracods and microbial deposits) as well as stable isotopes. In the following, we present a detailed investigation of the carbonate microfacies of the Baghuk Mountain section. We aim to decipher (1) biogenic and abiogenic carbonate production in the transition from the Palaeozoic to the Mesozoic, (2) indications of redox conditions in the Late Permian successions and the extinction horizon, (3) the trigger of carbonate formation in the Early Triassic and (4) indications of large-scale sea level changes or subaerial exposure in the study area. This study contributes to the understanding of the timing of the end-Baghuk Mountain is located in Central Iran, 140 km SSEmentological perturbations.

Previous work

Kuh-e-Hambast

Permian–Triassic boundary beds have already been intensively studied in sections at Kuh-e-Hambast (=Hambast

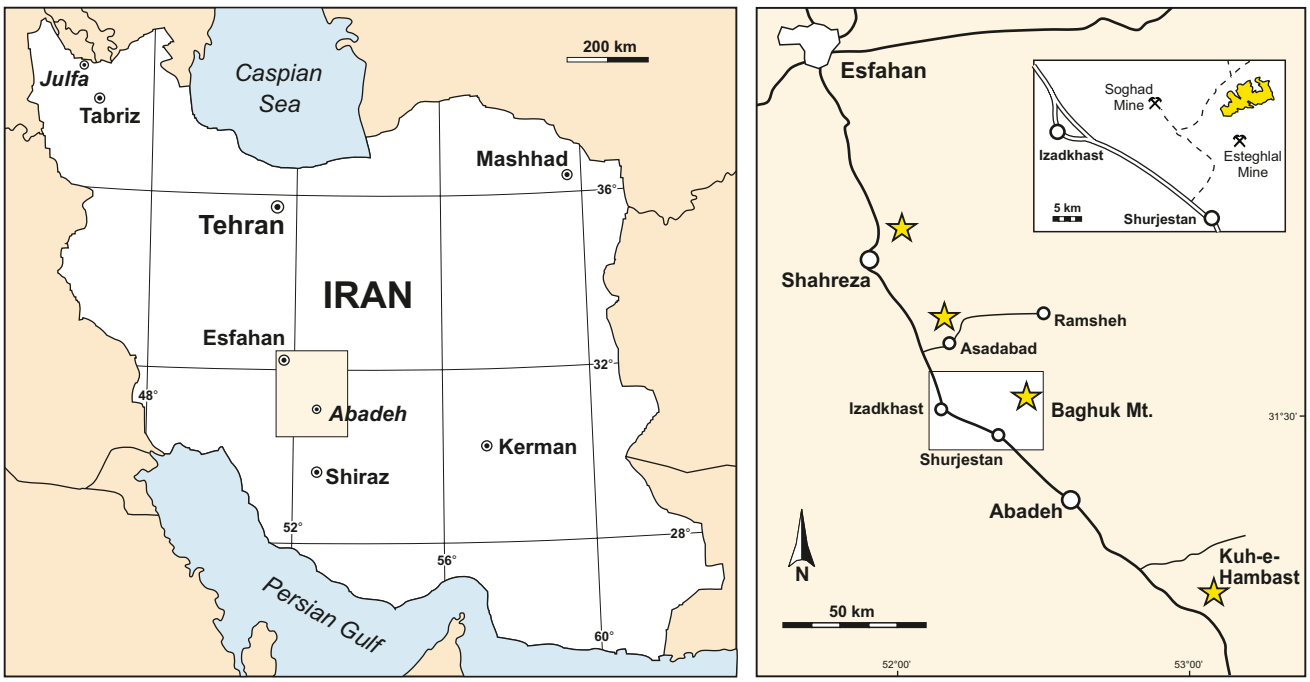

Fig. 1 Geographic position of the P-Tr boundary sections at Baghuk Mountain

Range; 60 km SE of Abadeh). The Late Permian to Early Triassic stratigraphy in this region was first outlined by Taraz (1969, 1974); he divided the Permian sedimentary succession into seven units (named units 1 to 7 in ascending order) and the Early Triassic succession into five units (units a to e). The Permian units were later assigned to three formations (Taraz et al. 1981), the Surmaq, Abadeh and Hambast formations in ascending order. The rock succession in the Hambast Range can serve as a standard for the Central Iranian sections of the Permian–Triassic transition.

The Late Permian Hambast Formation has a thickness of about 35 m at the type locality (Kuh-e-Hambast) and consists almost entirely of platy and nodular limestone beds (Taraz et al. 1981). The Late Permian Wuchiapingian (=Dzhulfian in their terminology) and Changhsingian (=Dorashamian) stages are, according to Taraz et al. (1981), represented in almost equal proportions. In the last five decades, a local lithostratigraphic scheme in combination with high-resolution conodont- and ammonoid-based biostratigraphy, geochemistry and event stratigraphy of the Permian–Triassic boundary layers has been developed (Taraz 1969, 1971, 1973; Bando 1979, 1981; Taraz et al. 1981; Baud et al. 1997; Besse et al. 1998; Gallet et al. 2000; Partoazar 2002; Kozur 2004, 2005, 2007; Horacek et al. 2007a, b; Richoz et al. 2010). Contradictory results with respect to the conodont stratigraphy were presented by Kozur (2005, 2007) and Richoz et al. (2010); the differences between the results were discussed and clarified by Horacek et al. (2021). Studies on the $^{18}O/^{16}O$ ratio of conodont apatite and resulting temperature changes across the Permian–Triassic boundary have been achieved by Chen et al. (2020) and led to the result that the main extinction was triggered by a sudden seawater warming.

These investigations demonstrated that the Late Permian to Early Triassic succession is very similar to the classical sections near Dzhulfa (Azerbaijan) and Julfa (NW Iran). The upper part of the Late Permian carbonate succession, which is equivalent with the *Paratirolites* Limestone of the Julfa area (Ghaderi et al. 2014; Gliwa et al. 2020) extends from the *Clarkina bachmanni* Zone to the *Clarkina hauschkei* Zone (Fig. 2).

The lithological succession and the environmental conditions of sections in the Hambast Range had been thoroughly investigated, interpreted and discussed by Heydari's working group (Heydari et al. 2000, 2003; Heydari and Hassanzadeh 2003). They described the argillaceous, light grey and bioturbated mudstone of the Late Permian unit 6 and the argillaceous, nodular mudstone and wackestone of unit 7 and proposed a deposition at a water depth between 100 and 200 m. According to their investigations, the latest Permian and earliest Triassic succession consists of three units in ascending order:

(1) The lowermost around 1.5 m thick unit is the 'Boundary Clay' (=Baghuk Member) with shales and aggregates of dome-shaped or botryoidal crystals ('calcite

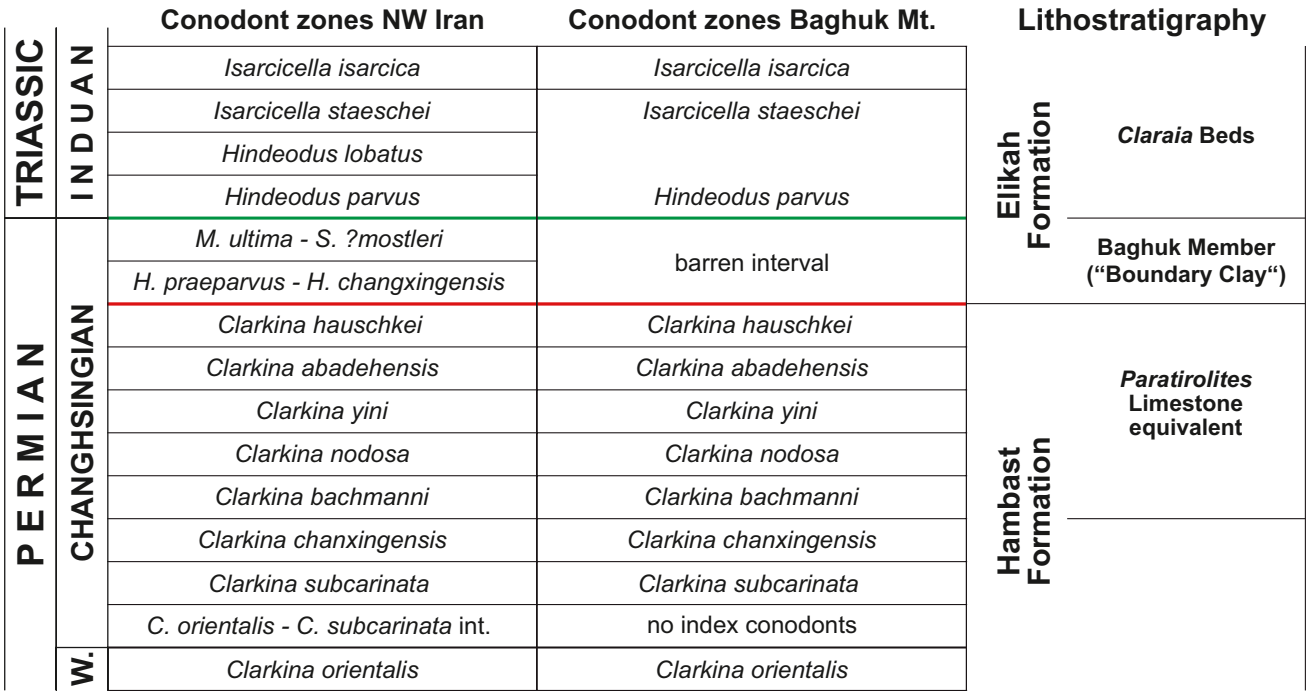

Fig. 2 Stratigraphic subdivision of the P-Tr boundary sections at Baghuk Mountain. Conodont stratigraphy of the Julfa region after Ghaderi et al. (2014) and Baghuk Mountain after Farshid et al. (2016) and Korn et al. (2021). W = Wuchiapingian

fans'), interpreted by Baud et al. (2021) as digitate stromatolites.

(2) The overlying unit of 1.5 m thickness is composed of packstone and grainstone with recrystallised grains, probably ooids or peloids.

(3) The third Early Triassic, more than 100 m thick, unit is described as thin-bedded, bioturbated to nodular limestone with specimens of *Claraia*.

Heydari et al. (2001) focused on the lithological succession and the $\delta^{13}C_{carb}$ as well as the $\delta^{18}O$ signatures of the Hambast section. Subsequently, carbon and strontium isotope geochemistry has been carried out by other research groups (Korte et al. 2004a, b, 2010; Horacek et al. 2007a, b; Richoz et al. 2010; Liu et al. 2013).

Mohtat-Aghai and Vachard (2005) paid attention to the Late Permian to Early Triassic foraminifer biostratigraphy in the Hambast region. They also described various lithological features and concluded that there is a shift from an 'ammonitico rosso' facies to a facies conspicuous for the occurrence of microbialites.

Shahreza

The Permian–Triassic boundary exposure 14.5 km NNE of Shahreza (Fig. 1) shows a succession that is rather similar to the sections in the Hambast Range. The Hambast Formation at Shahreza consists primarily of nodular, often bioturbated limestones which were deposited in deep water below the storm wave. The P–T boundary interval consists of red shale, interpreted as terra rosa, which was formed during subaerial exposure (Heydari et al. 2001, 2008).

The Late Permian sedimentary rocks are overlain by the Elikah Formation (named Shahreza Formation by Heydari et al. 2008, 2013), which consists of grainstone, packstone and microbial mounds that may represent a shallow subtidal to intertidal facies. The microbial mounds are composed of radial fans of calcite crystals (Heydari et al. 2008). These authors suggested that the calcite deposits are formed by synsedimentary carbonate precipitation and proposed a model for the lithological change caused by increasing carbonate saturation of seawater. Baud et al. (2007) described branched, thinly laminated microbialites from Shahreza and compared them with Late Proterozoic stromatolites. The 'calcite fans' in the Shahreza section were interpreted by Richoz et al. (2010) as fans precipitated on the sea floor. The conodont zonation in the Shahreza section was outlined in combination with the signatures of $\delta^{13}C_{carb}$ (Korte et al. 2004a, b; Kozur 2007; Heydari et al. 2008; Richoz et al. 2010; Schobben et al. 2017).

Baghuk Mountain

Permian–Triassic boundary beds at Baghuk Mountain were probably first studied by Ghaedi et al. (2009), who used the name Benarizeh for the section. These authors separated between three biozones, from bottom to top *Pseudogastrioceras* beds, *Paratirolites* beds and *Claraia* beds and correlated them with the succession known from Julfa, Shahreza and Abadeh. Ghaedi et al. (2009) illustrated a microbialite that was regarded as "algal remains".

Late Permian chondrichthyan and actinopterygian fishes from Baghuk Mountain were reported by Hampe et al. (2013). Leda et al. (2014) outlined the lithology and a brief microfacies description of one of the Baghuk Mountain sections and compared the results with sections near Julfa (NW Iran). They focused on the topmost Hambast Formation (*Paratirolites* Limestone equivalent), the Baghuk Member and the *Claraia* Beds. Leda et al. (2014) described Early Triassic 'calcite fans' similar to the ones described earlier by Heydari et al. (2008) from Kuh-e-Hambast and Foster et al. (2020) discussed the microbialites of Baghuk Mountain in a global framework.

Localities

Baghuk Mountain is located in Central Iran, 140 km SSE of Esfahan and 45 km NNW of Abadeh (Fig. 1). Palaeogeographically, the outcrop area is part of the Sanandaj-Sirjan Zone on the Cimmerian Microcontinent, near the equator on the Neotethyan shelf (Stöcklin 1968; Nabavi 1976; Stampfli and Borel 2002, 2004; Torsvik and Cocks 2004) (Fig. 3). However, there is ongoing discussion about the palaeogeographic setting of the Cimmerian Microcontinent (Ruban et al. 2007).

For the microfacies, we intensely studied two sections at Baghuk Mountain, located about 100 m apart:

Baghuk Mountain 1 Sect. (31.5675°N, 52.4436°E) – The samples from Sect. 1 represent the upper twelve metres of the Late Permian Hambast-Formation.

Baghuk Mountain C Sect. (31.5671°N, 52.4428°E) – We used the samples from section C to describe the microfacies of the uppermost four metres of the Hambast-Formation and the lowest 25 m of the Early Triassic Elikah Formation.

The excellent outcrop conditions at Baghuk Mountain enabled detailed sampling across the Permian–Triassic boundary (Fig. 4). In order to obtain a detailed picture of the various lithological features across the Permian–Triassic boundary, the samples were taken at centimetre range, i.e. with the best possible stratigraphic resolution.

The stratigraphic position of the samples is documented in alignment with the position of the extinction horizon, which is characterised by the sharp contact, visible as a sudden change from reddish nodular limestones to dark-grey shales,

Fig. 3 Palaeogeographic positon of the Baghuk Mountain area from the Late Permian to Early Triassic (after Stampfli and Borel 2002, 2004)

between the Hambast-Formation and the Baghuk Member. Samples from above the extinction horizon are marked with a plus prefix (+), samples from below with a minus prefix (-).

Lithostratigraphy

The sections at Baghuk Mountain show facies changes across the Permian–Triassic transition, on which several formations were defined (Taraz et al. 1981) (Fig. 5). We studied three lithostratigraphic units:

(1) Hambast Formation. – The formation is characterised by grey (in the lower part; thickness 16 m) or red (in the upper part; thickness 18 m) platy or nodular and occasionally marly limestone beds, which form packages with a thickness of 0.10 m to 0.50 m. In the upper part of the formation there are two lithological index horizons that can be used for correlation between the sections: (a) A conspicuous red shale horizon, 0.20 to 0.40 m thick, accompanied by red nodular limestone beds; this occurs in all sections about five metres below the extinction horizon. It shows an accumulation of the ammonoid genus *Shevyrevites* (Fig. 5) and can be correlated with the upper part of the Zal Member just below the base of the *Paratirolites* Limestone of NW Iran (Ghaderi et al. 2014; Korn et al. 2019; Gliwa et al. 2020). (b) A compact reddish-brown limestone bed with a thickness of 10 to 20 cm with poor macrofossil content occurs at -3.20 to -3.50 m.

Fig. 4 The Permian–Triassic boundary section in Baghuk Mountain section C. View towards the West; thickness of the Baghuk Member is two metres

(2) Baghuk Member ('Boundary Clay') (Korn et al. 2021). – Above the Hambast Formation follows, with a sharp lithological contact, the approximately two metres thick Baghuk Member. Although this represents the youngest Changhsingian, it already belongs to the Elikah formation. The Baghuk Member reflects the sedimentological and ecological condition immediately after the main extinction pulse. The unit consists of brittle grey shales with so-called 'calcite fans' (digitate stromatolites according to Baud et al., 2021) in the upper part. These calcite structures are embedded in a matrix containing sponge remains. The 'calcite fans' are laminated and show botryoidal and leaf-shaped crystal growth.

(3) *Claraia* Beds. – Most of the basal part of theElikah Formation consists of thin, platy limestone beds that begin directly above the Baghuk Member. Thin platy limestone beds, shales with a thickness of up to 0.30 m and compact limestone beds with a thickness of up to 0.20 m form this rock unit. Higher

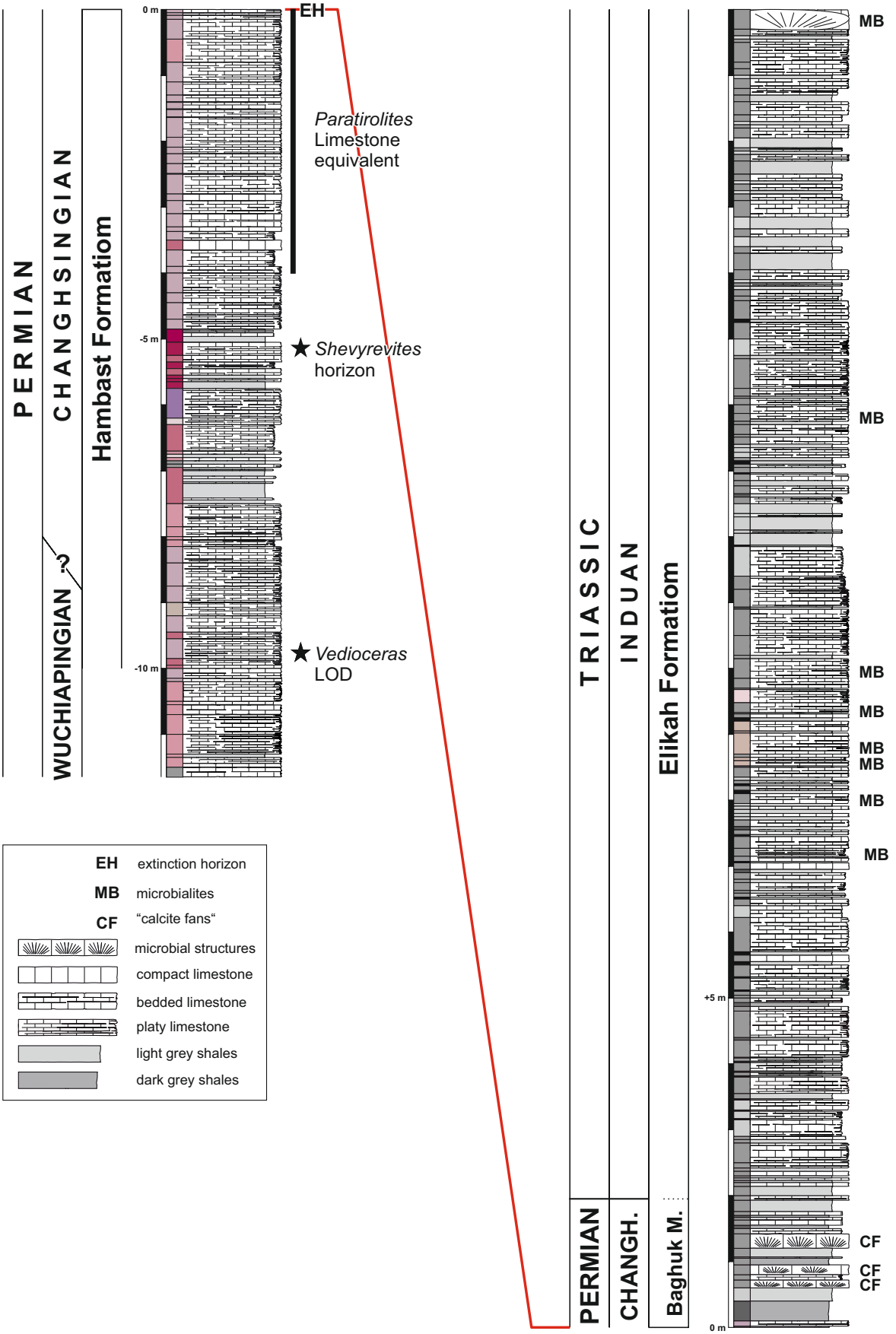
PERMIAN
CHANGHSINGIAN
WUCHIAPINGIAN
?
Hambast Formation
0 m
-5 m
-10 m
EH
Paratirolites
Limestone
equivalent
Shevyrevites
horizon
Vedioceras
LOD
EH extinction horizon
MB microbialites
CF "calcite fans"
microbial structures
compact limestone
bedded limestone
platy limestone
light grey shales
dark grey shales
TRIASSIC
INDUAN
PERMIAN
CHANGH.
Elikah Formation
Baghuk M.
MB
MB
MB
MB
MB
MB
MB
MB
+5 m
CF
CF
CF
0 m

◂**Fig. 5** Columnar sections of the Permian Triassic boundary at Baghuk Mountain with characteristic lithological units and index horizons. Hambast Formation measured in Sect. 1, Elikah Formation measured in section C (after Korn et al. 2021)

parts of the *Claraia* Beds up to + 48.00 m consist of platy limestone beds with thin shale intercalations. This succession includes microbial deposits at several levels and of various morphological types, all of which are associated with sponge remains. Many of the microbialite structures are accompanied by specimens of the bivalve *Claraia*.

Carbonate microfacies

Methods

About 140 thin sections were produced in the Museum für Naturkunde Berlin (Germany) and at the Buali-Sina University of Hamedan (Iran)to systematically study the fossil content, non-skeletal grains and sedimentary structures. Additionally more than 90 polished slabs were prepared for the morphological study of the microbialites. The thin sections were used for the microfacies analysis, including the presence and amount of biogens and taphonomic features. A detailed petrographic analysis was achieved with a polarizing microscope of the type Zeiss Axioskop 40 fit with a digital camera (Zeiss AxioCam MRc5) working with Axio Vision LE software.

Identified facies were compared with standard microfacies types (SMF) (e.g. Wilson 1975; Burchette and Wright 1992; Flügel 2013). Depositional environments of the carbonate facies were discussed based on their petrographic characteristics (Flügel 2013). Concerning nomenclature, this paper follows the definitions and descriptions of microbial limestones presented by Shapiro (2000), who used different categories to describe the microbial fabric (mega-, macro-, meso-, and microstructural). We use the term microbialite (Burne and Moore 1987) as an overall term for all microbial structures.

Semi-quantitative analyses of biogen frequencies were performed using comparison tables of Baccelle and Bosellini (1965). We used five degrees of occurrence frequency: absent, extremely rare, infrequent, moderately frequent and frequent. The degree of bioturbation was determined semi-quantitatively according to Reineck (1967), Droser and Bottjer (1986) and Taylor and Goldring (1993). We interpreted the depositional area and palaeoenvironment using the model of the Standard Facies Zone (Wilson 1975; Schlager 2002).

Microfacies description

Hambast Formation

Microfacies HF1 – weakly bioturbated ostracod wackestone/packstone (Fig. 6a, b)

Occurrence: Most common at the top of the Wuchiapingian and the base of the Changhsingian part of Hambast Formation between -9.90 m and -7.50 m.

Depending on the content of allochems, this microfacies is a mud-supported wackestone or a grain-supported packstone. In both cases it contains abundant well-preserved and also disarticulated thin-shelled ostracod valves without preferred orientation; the percentage of skeletal grains ranges from 10 to 85%. The reddish or greyish matrix is composed of microsparite; it shows diagenetic textures including pressure solution seams as well as calcite veins. Some areas of the matrix are recrystallised; others are affected by iron precipitation. Mainly equigranular, hypidiotopic crystallization fabrics replaced the microsparite matrix. Burrows of various shapes are rare; they are filled with light-grey fine-grained micrite to microsparite without biogenic components. Contacts between burrow margins and the surrounding matrix are either sharp or indistinct. Biogenic components in this facies are crinoid arm plates and other echinoderm fragments with recognisable stereom, calcispheres and radiolarians, partly dissolved fragments of ammonoids and other molluscs. Ostracod valves of sculptured and smooth-shelled species are filled with the surrounding matrix or sparitic cement; nearly all specimens have a similar size (0.5 mm length). A few euhedral mineral grains, probably pyrite and hematite, and extremely rare dark green, subangular crystals, probably chlorite, occur rarely in this microfacies.

Microfacies HF2 – moderately bioturbated nodular mudstone/wackestone (Fig. 6c, d)

Occurrence: Lower part of the Changhsingian part of the Hambast Formation between -7.50 at -4.40 m.

The limestone beds possess a conspicuous nodular fabric; the nodules have rounded to irregular outlines and are composed of microsparite. They differ in the lighter colour from the surrounding marly matrix. A few nodules are bordered by pressure solution seams. The microsparite matrix has a grey to conspicuously red colour. Most of the contacts between nodules and shale matrix are indistinct, indicating a formation affected by bioturbation and diagenetic overprint (compare Flügel 2013). An interconnected burrow network is composed of irregular burrows. Biogenic components are sponge spicules, echinoderm remains with preserved stereom, bivalves, ammonoids, brachiopods, ostracods, radiolarians and

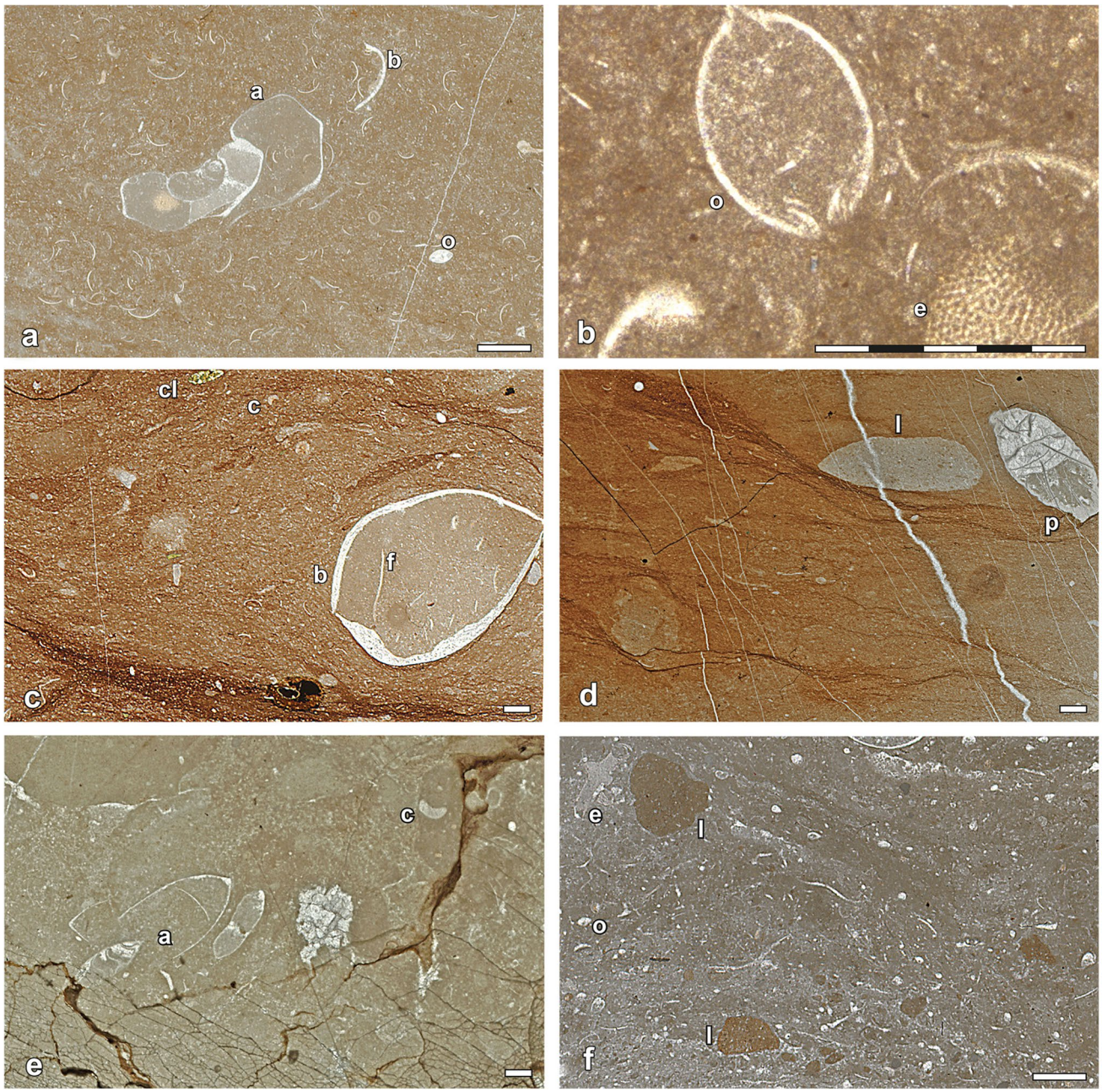

Fig. 6 Microfacies of the Late Permian Hambast Formation in Baghuk Mountain Sect. 1 (scale bar units for a, c-f = 1 mm; scale bar units for b = 0.1 mm). **a** Microfacies HF1: Ostracod wackestone/packestone dominated by thin-shelled, well-preserved ostracods and disarticulated valves, filled with sparitic cement (o), ammonoid (a) filled with grey muddy matrix, which is grey micritic matrix and small shell fragments, disarticulated bivalve shell (b); -9.90 m. **b** Microfacies HF1: Ostracod wackestone/packestone with well-preserved smooth-shelled ostracod (o) in a red fine-graind matrix with preservation allowing recognition of the duplicature, echinoderm (e) fragment with stereom preservation; -9.90 m. **c** Microfacies HF2: Red nodular argillaceous mudstone/wackestone; micritic matrix partly recrystallised and affected by pressure solution. A well-preserved articulated brachiopod (b) filled with fine-grained matrix and filament fragments (f), lunate crinoid arm plates (c) and chlorite crystals (cl); -6.25 m. **d** Microfacies HF2: Weakly bioturbated red mudstone/wackestone with single rugose solitary coral *Pentaphyllum* (p) and a subrounded light grey lithoclast (l); -4.80 m. **e** Microfacies HF3: Partly recrystallised micritic matrix with pseudopeloidal texture, poorly preserved ammonoids (a) and lunate crinoid arm plats (c); -2.45 m. **f** Microfacies HF3: Grey, partly recrystallised micritic matrix with irregularly shaped lumps of carbonate mud (l), ostracods (o) and echinoderms (e) floating in the matrix; -1.20 m.

indistinctive shell fragments. The majority of the biogens are small, reaching a size of only 1 mm. The ammonoid conchs are widely dissolved with inner volutions filled with sparitic cement; thin-shelled ostracod valves are filled with matrix or sparitic cement. Diagenetic features are numerous pressure solution seams that generate stylonudular and stylobreccioid structures, calcite veins and microfractures. A rare feature is the occurrence of euhedral opaque mineral grains, presumably pyrite and hematite, as well as dark-green subrounded chlorite grains.

Microfacies HF3 – weakly bioturbated mudstone/wackestone (Fig. 6e, f)

Occurrence: Upper part of the Hambast Formation below the extinction horizon, particularly the top above -0.40 m. Similar facies, however, is present in the upper part of the Hambast Formation beginning at -4.40 m.

This microfacies is characterised by a fine-grained micritic to microsparitic matrix, a low bioturbation degree and sparse biogenic content. At a level of -2.45 m, the matrix has a pseudopeloidal texture. The biogenic content of this facies consists of ammonoids, ostracods, crinoids and other echinoderms, radiolarians, bivalves, rare foraminifera and indistinctive shell fragments. Radiolarians of the order Entactinaria can be identified (W. Kiessling, personal comm.) as well as a single rugose coral of the genus *Pentaphyllum* (D. Weyer, personal comm.). The majority of biogens are poorly preserved, except from few well-preserved crinoid remains. The original aragonite of the ammonoid septa was recrystallised to calcite and the phragmocone chambers were filled with blocky cement. Ostracod valves are filled with matrix or sparite cement, which in some cases show geopetal orientation. Other shells are partially dissolved and affected by dark incrustations. Red to brown subangular lithoclasts are rare. Diagenetic features include single vertical and horizontal cracks filled with micrite and blocky cement. Irregular anastomosing pressure solution sets and bedding-parallel irregularly sutured seams with small to large amplitude are sometimes horsetail-structured. They generated stylomottled pressure solution structures (compare Flügel 2013). Iron dendrites and a few euhedral mineral grains (probably pyrite or hematite) occur frequently.

Baghuk Member

Microfacies BM1 – weakly bioturbated fossiliferous mudstone/wackestone (Fig. 7a)

Occurrence: Grey limestone nodules at the base of the Baghuk Member in section C.

Components of these microfacies are embedded in a reddish to greyish lime mud matrix, which is partly affected by neomorphism; many widespread Fe dendrites are common. Irregular burrows are rare in this facies; they are filled with the surrounding matrix. The biogenic inventory consists of bivalves, ostracod valves and indistinct shell fragments. Thin-shelled ostracod carapaces are filled with micrite or sparitic cement. Calcite fillings in microcracks and microfractures as well as irregularly anastomosing stylolite sets are common. The heavy mineral content is composed of euhedral pyrite or hematite grains.

Microfacies BM2 – sponge wackestone with 'calcite fans' (Fig. 7b-d)

Occurrence: At + 0.55 m and + 0.75 m in section C and irregularly distributed in the Baghuk Member in parallel sections.

This microfacies shows a dense accumulation of sponge spicules and the appearance of 'calcite fans', identified as digitate stromatolite by Baud et al. (2021), in a fine-grained grey to reddish micritic matrix with scattered Fe incrustations. Sponge remains of keratose demosponges occur in different morphologies; they can be identified as monoaxons and triaxons, but there is also a dominant proportion of irregular and unclassifiable remains. Various types of cement growth and cement generations accompany the 'calcite fans'; they occur in stratified and radiaxial fibrous structures, partly growing on top of each other. Diagenetic features include pressure solution seams with a brecciated structure. Individual thin calcite veins penetrate both the digitate stromatolites and the surrounding matrix.

Microfacies BM3 – weakly bioturbated marly siltstone with grey marly nodules

Occurrence: Middle part of the Baghuk Member.

Within the reddish marly matrix of siltstone, the biogenic assemblage is composed of few ammonoids, thin-shelled ostracods and indistinctive shell fragments. The biogenic content of grey marly nodules is made up of sponge spicules, consisting of monoaxons, triaxons, irregular and non-allocate specimens. Few burrows are filled with dark brown micrite, unlike the surrounding matrix. The matrix is affected by small, widespread Fe-dendrites.

Claraia Beds

Microfacies CB1: Laminated wackestone/mudstone with calcite spheres (Fig. 8a)

Occurrence: Base of the *Claraia* Beds at + 2.45 m and + 5.45 m.

This facies is characterised by greyish to brown mudstone or wackestone with sparry, neomorphic components. The laminated fabric consists of millimetre-thick lamellae, which

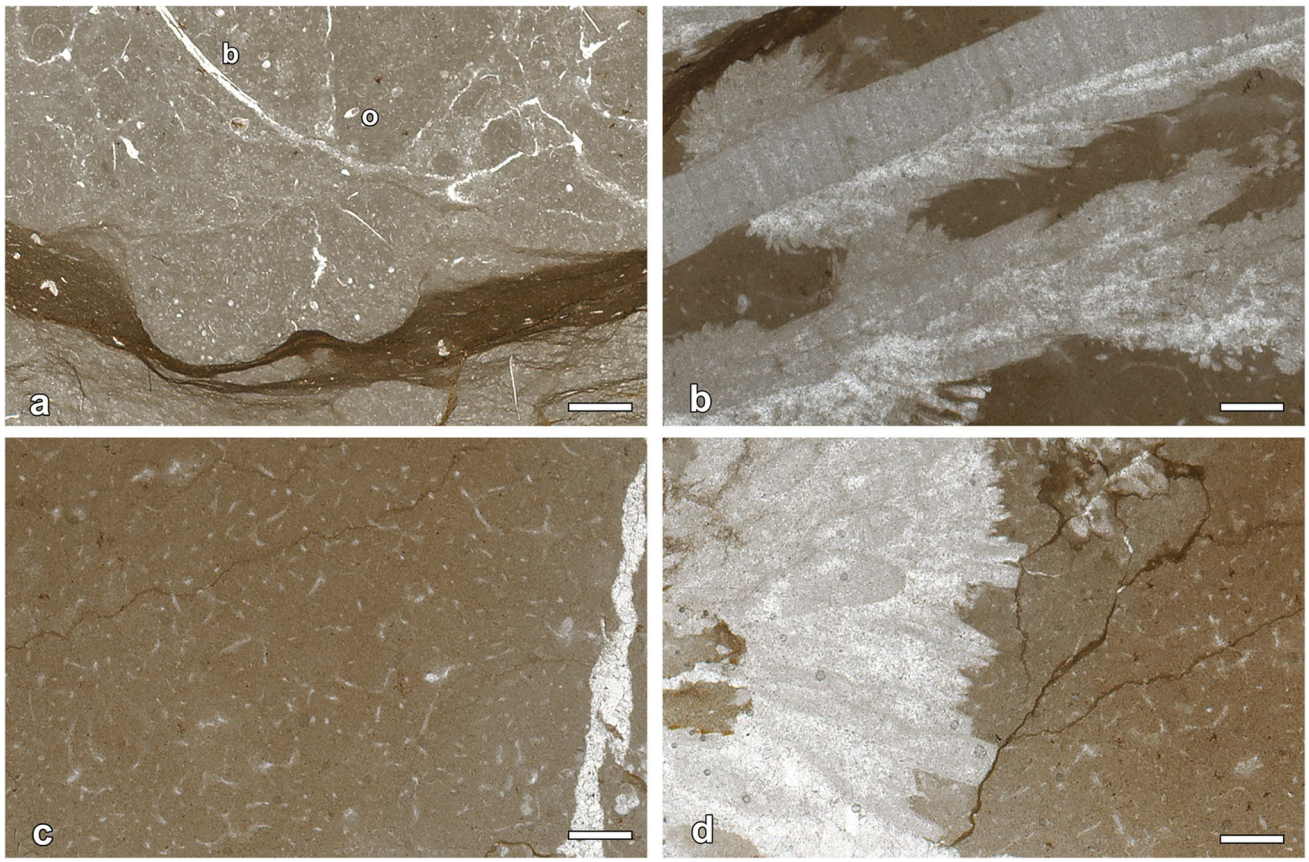

Fig. 7 Microfacies of the Baghuk Member in Baghuk Mountain section C; scale bars = 1 mm. **a** Microfacies BM1: partly neomorphosed fossiliferous mudstone to wackestone with irregular anastomosing stylolite sets. A large bivalve shell (b) and ostracods (o) float inside the grey matrix; + 0.02 m. **b** Microfacies BM2: Sponge wackestone with 'calcite fans', laminated 'calcite fans' with botryoidal and bladed crystal growth in reddish sponge wackestone; + 0.75 m. **c** Microfacies BM2: Detail of the reddish sponge wackesteone matrix. Various morphologies of sponge remains occur inside the micritic matrix. Monoaxons and triaxons can be identified, but there is also a dominant proportion of irregular and non-allocateable remains. The siliceous sponge spicules were dissolved and replaced by calcite; + 0.55 m. **d** Microfacies BM2: 'calcite fans' growing inside the red sponge wackestone matrix; + 0.55 m

differ in their internal composition. Slightly thicker lamellae consist of closely spaced sparry spheres, which vary in size and morphology ranging from irregular to euhedral. In some beds, the calcite spheres are normally graded and cause layers separated by different grain size. Fine-grained components are formed by individual calcite crystals. Coarser components are accumulations of several individual calcite grains or single grains. The lowest layer is separated from the lime mud matrix by the bedding of parallel pressure solution seams. Biogens are rare and consist of few micrite-filled ostracod valves and small shell fragments. Swarms of pressure solution seams cross the matrix. Some horsetail structures and calcite veins are visible.

Microfacies CB2 – laminated mudstone (Fig. 8b)

Occurrence: *Claraia* Beds between + 6.60 m and + 48.00 m.

The microfacies shows wispy to broad lamination that is characterised by a colour change form light grey to darker grey. The matrix is fine-crystalline micrite without any grain size change. Some parts of the matrix are recrystallised. Diagenetic features are calcite veins and single stylolites.

The laminated mudstone was deposited in a low-energy environment with quiet water conditions below storm wave base in a restricted marine area.

Microfacies CB3 – bivalve and ammonoid sponge wackestone with microbial structures (Fig. 8c, d)

Occurrence: *Claraia* Beds, best developed between + 8.55 m and + 18.85 m.

This facies is a burrowed wackestone with domal, dish-shaped microbial overgrowth on bivalve and ammonoid shells. The thin section from + 13.95 m contains a large ammonoid conch as well as thin bivalve shells with layered microbial overgrowth. The aragonitic ammonoid shell is completely neomorphosed; the initial whorls as well as part of the outer chambers are filled with blocky sparite; other parts of the

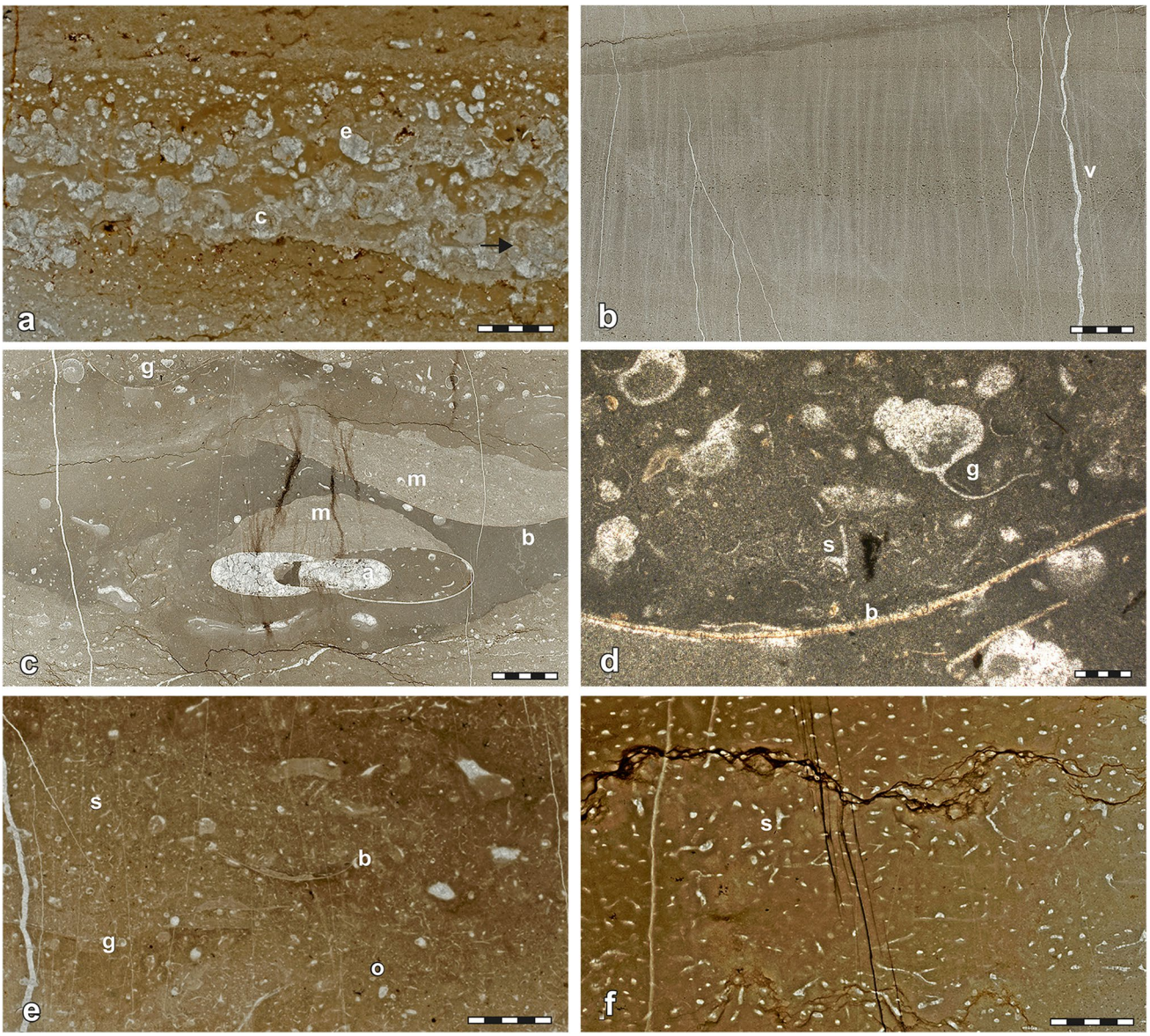

Fig. 8 Microfacies of the Early Triassic *Claraia* Beds of the Elikah Formation in Baghuk Mountain section C (scale bar units for a-c, e, f = 1 mm; scale bar units for d = 0.1 mm). **a** Microfacies CB1 Greyish to brown mudstone to wackestone with calcite spheres (e) and recrystallised, restored components (c), laminated fabric of millimetre-thick laminae that differ in their internal composition, fine-grained components formed by single calcite crystals, coarser components are accumulations of several single calcite (arrow) grains or single grains; + 5.45 m. **b** Microfacies CB2: Laminated mudstone without any biogens, matrix partly recrystallised; + 48.00 m. **c** Microfacies CB3: Burrowed wackestone with microbial overgrowth. An ammonoid conch (a) with phragmocone filled with blocky sparite and body chamber filled with micritic matrix, thin bivalve shells (b) with layered microbial overgrowth (m) and numerous gastropod shells (g); + 13.95 m. **d** Microfacies CB3: detail of c) with brownish bivalve shells (b) and small gastropods (g), single sponge spicules (s) float in the matrix; + 13.95 m. **e** Microfacies CB4: red sponge wackestone with small, thin, densely packed sponge spicules, various morphologies of keratose demosponge remains (monoaxons and triaxons) (s) in micritic matrix, furthermore gastropods (g), bivalves (b) and ostracods (o), burrows partly recrystallised; + 10.50 m. **f** Microfacies CB4: sponge wackestone with widespread sponge remains (s); + 14.80 m

conch are filled with matrix. The interspaces between bivalve shells are filled with matrix containing abundant sponge spicules. Additionally, gastropods and ostracods are part of the biogenic content of this facies. The bioturbation is weak and characterised by partly recrystallised, burrows. Calcite veins as well as single sutured and non-sutured stylolites cross the matrix. Occasionally, large bivalve shells occur in chaotic position (convex-up and convex-down).

Microfacies CB4 – sponge wackestone/packstone (Fig. 8e, f)

Occurrence: *Claraia* Beds between + 10.50 m and + 13.60 m.

This facies is characterised by a reddish fine-grained micritic matrix with a dense accumulation of sponge spicules with various morphological features (keratose demosponges); the sponge spicules are monoaxons and triaxons and a dominant proportion of irregular and non-allocateable remains. The sponge remains range, in their morphology, from small, thin densely packed spicules to big, broad and widespread clusters. The amorphous silica of the spicules has been completely replaced by calcite, so that they are preserved as calcite pseudomorphs (Leda et al. 2014).

Microfacies CB5: Microbialitic structures

Occurrence: Various levels in the *Claraia* Beds between + 8.55 m and + 19.70 m.

The microbialites at Baghuk Mountain are diverse in scale, external morphology and internal structure (Fig. 9). Three macroscopic morphotypes are distinguished here: (1) dome-shaped, conical and/or bulbous in shape with protuberance on top and round to ellipsoid form, (2) planar and lens- to dome-shaped with protuberance on top and (3) club-shaped and mushroom-shaped, inverted conical structures with dished upper surface. Common mesostructures are dendrolite (dendritic), stromatolite (laminated), thrombolite (clotted) or leiolite (structureless, aphanitic). Club-shaped microbialites were regularly growing on bivalve or ammonoid shells as solitary structures or small communities. Thin section investigation reveals that various microbialites are accompanied with keratose demosponges.

Depositional history, biogenic content and bioturbation degree

Hambast Formation

The microfacies analysis of the top 10 m of the Late Permian Hambast-Formation enables a reconstruction of the latest Wuchiapingian and Changhsingian carbonate environment of the time before the main extinction pulse. Both the biogenic content and the degree of bioturbation provide information about the likely oxygen supply to the seafloor (Fig. 10, 11).

The sediments of the Wuchiapingian-Changhsingian boundary interval (-9.90 m to -7.50 m) contain mostly benthic organisms and show little evidence of bioturbation. Radiolarians, echinoderms and cephalopods indicate a fully marine, normal saline environment. The high proportion of non-oriented ostracods and the bimodal ratio of complete shells and single disarticulated valves may indicate deposition in an episodic high-energy environment. Similar time-equivalent deposits with mass occurrences of ostracods are already known from Ali Bashi near Julfa in NW Iran (Baud 2008; Leda et al. 2014).

The Changhsingian record from our sampled sections contains mainly benthic organisms, occurring in ostracod packstone, non-fossiliferous mudstone and sparse to moderately bioturbated mudstone to wackestone. They reflect a mixed benthic and pelagic assemblage (ammonoids, ostracods, foraminifers, echinoderms, radiolarians, bivalves, sponges). A nodular mudstone to wackestone facies is present between -7.55 m and -5.95 m. It is the most common lithology in the upper part of the Hambast Formation and has already been described from several Late Permian sections in Central Iran (e.g. Taraz et al. 1981; Heydari et al. 2000, 2003; Mohtat-Aghai and Vachard 2005; Leda et al. 2014) as well as from time equivalent sections in the Julfa area (e.g. Stepanov et al. 1969; Teichert et al. 1973; Leda et al. 2014; Gliwa et al. 2020). The biogenic content of a mixed benthic and pelagic community speaks for a well-oxygenated environment. In contrast to Taraz et al. (1981), who proposed a lagoonal environment for these deposits, we agree with Heydari et al. (2000), Heydari et al. (2003) and Leda et al. (2014) and Gliwa et al. (2020), who interpreted the depositional environment as deep shelf setting below the storm wave base.

This nodular facies resembles the so-called Griotte Limestone of the Devonian and Carboniferous (e.g. Tucker 1974; Wendt and Aigner 1985; Baud and Richoz 2019) and the Jurassic Alpine-Mediterranean Ammonitico Rosso facies, which describe reddish to grey, nodular pelagic limestone formations with abundant ammonoids (e.g. Aubouin 1964; Garrison and Fischer 1969; Jenkyns 1991; Cecca et al. 1992; Mohtat Aghai et al. 2009). Mohtat Aghai et al. (2009) associated this facies with a decrease of $CaCO_3$ sedimentation and reduced oceanic circulation. Noble and Howells (1974) and Jenkyns (1991) postulated that the formation of the nodules is an early diagenetic process. Jenkyns (1991) suggested a rhythmic formation of the nodules based on dissolution of aragonite, leading to high carbonate concentrations at the sediment–water interface. According to this interpretation, the nodules were cemented directly below the sediment surface; they might have grown from skeletal calcite and micrite intraclasts, which acted as nuclei. Mamet and Préat (2006) discussed three formation scenarios for the red pigmentation of this facies. They concluded that the red colour is induced by oxidising iron microbes in a poorly oxygenated environment. In contrast, Heydari et al. (2003), Kozur (2007) and Leda et al. (2014) postulated that the reddish nodular limestone originated in a well-oxygenated environment, indicated by the specific biogenic content (e.g. ostracods) as well as the high bioturbation activity.

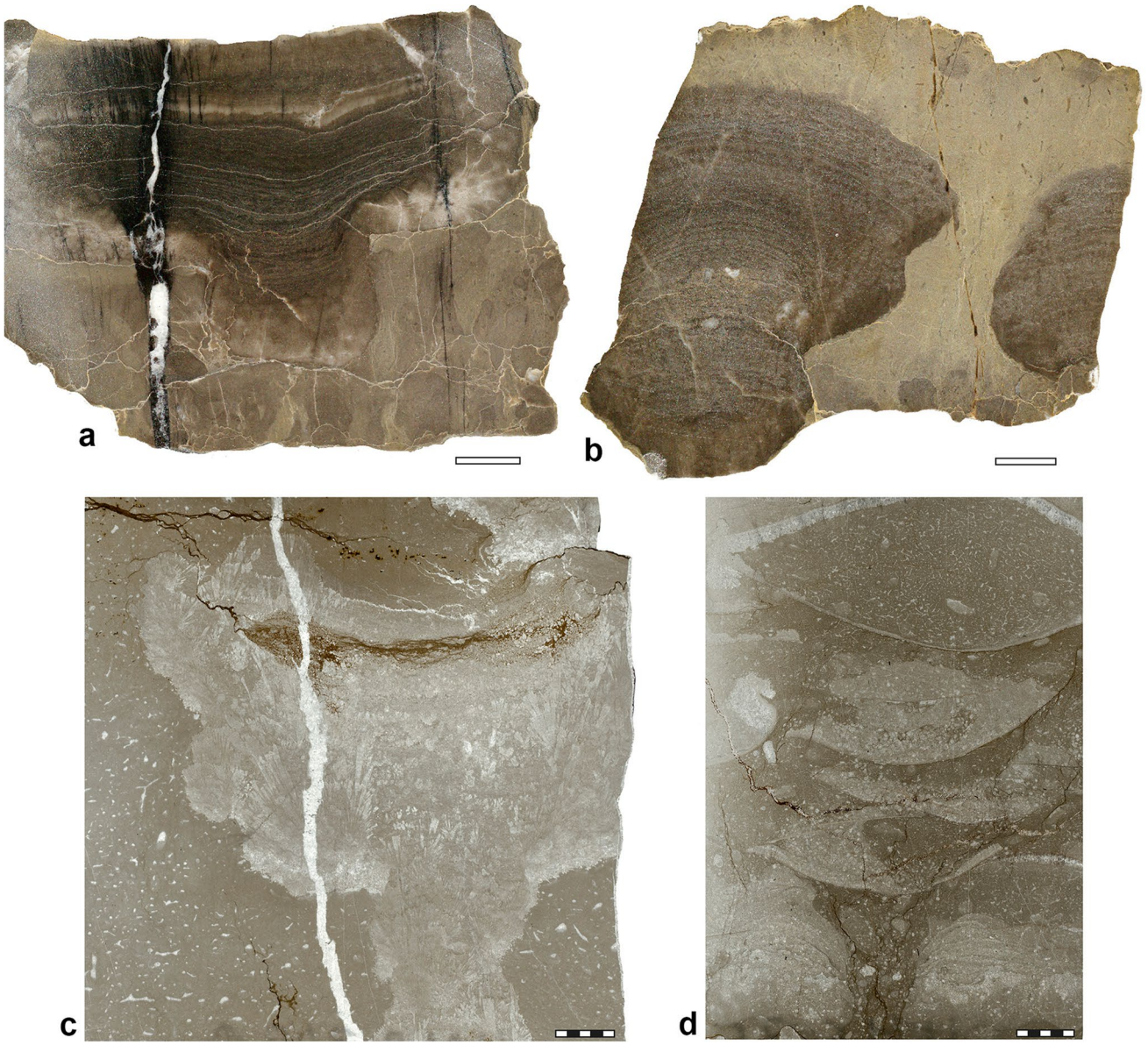

Fig. 9 Microfacies of Early Triassic microbialitic structures of Baghuk Mountain section C (scale bar units for a, b = 10 mm; scale bar units for c, d = 1 mm). **a** Polished rock sample of a "mushroom"-shaped microbialite; + 8.55 m. **b** Polished rock sample of a club-shaped microbialite; + 8.55 m. **c** Thin section of the "mushroom"-shaped microbialite of Fig. 9a; + 8.55 m. **d** Thin section of planar microbialites growing on bivalve shells; the surrounding matrix contains a high accumulation of sponge spicules; + 8.70 m

No evidence for discontinuity surfaces was seen throughout the entire Late Permian succession and therefore no break in sedimentation or deposition is recorded. Typical indicators like hardgrounds are missing.

The biogenic content and bioturbation of the Hambast Formation show a change from a predominantly benthic community with ostracods and echinoderms and only a few pelagic organisms (ammonoids and radiolarians) to a balanced mixed benthic and pelagic community (Fig. 10).

Ostracods and undifferentiated shell fragments are generally the most common bioclasts in the upper part of the Hambast Formation. The radiolarians show frequency fluctuations throughout the Changhsingian samples; they have already been described from time-equivalent strata of the Canadian Arctic and South China (Beauchamp and Baud 2002; Isozaki et al. 2007). Radiolarians are frequent in the interval between -9.90 m and -5.95 m and less common between -5.95 m and -2.00 m. In the topmost two metres of the Hambast Formation, they occur

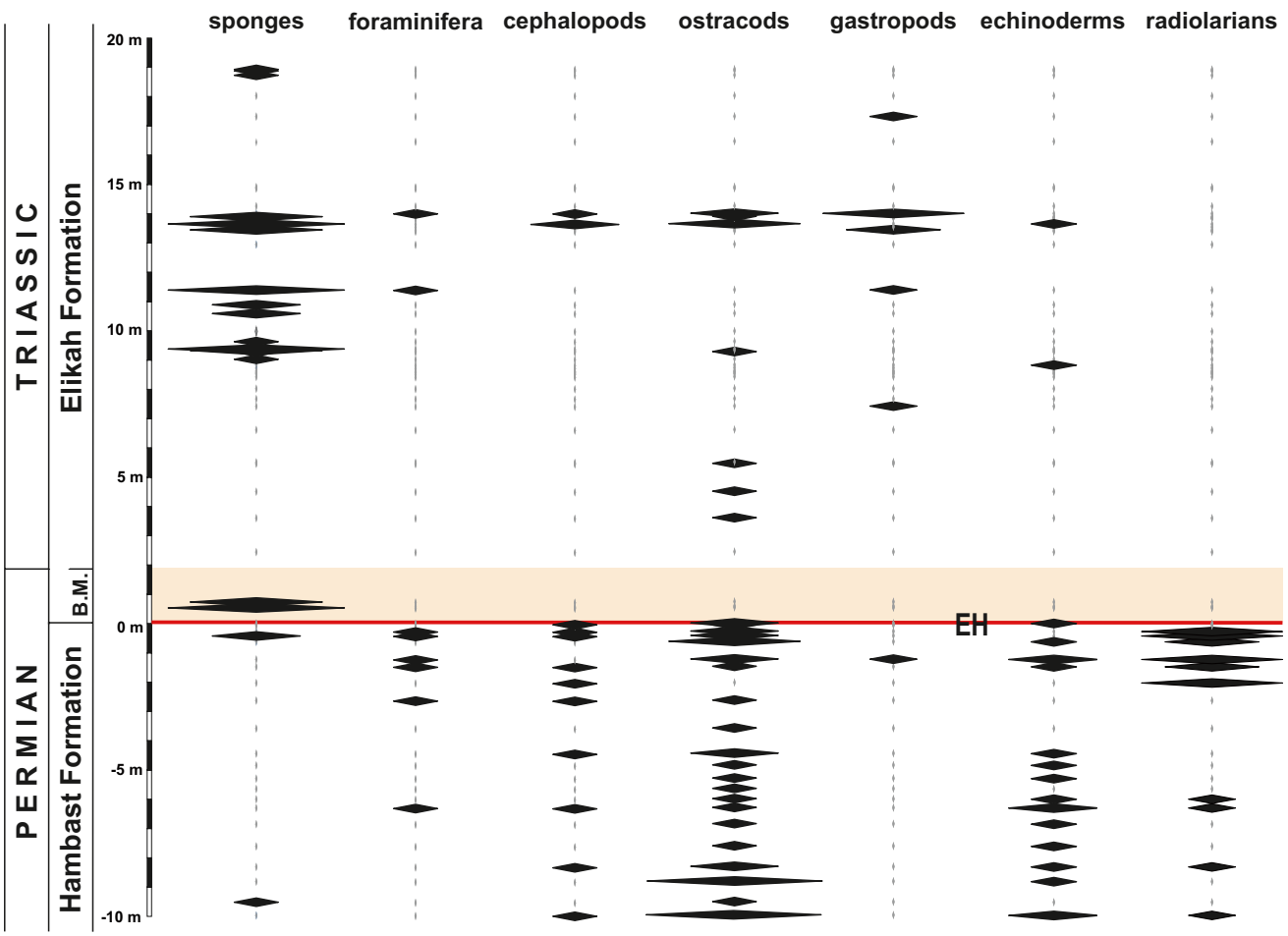

Fig. 10 Semi-quantitative frequency of selected biogens across the Permian–Triassic boundary in Baghuk Mountain Sect. 1 (Hambast Formation) and section C (Elikah Formation). B.M. = Baghuk Member

almost continuously in mass occurrences. Beauchamp and Baud (2002) suggested a collapse of biogenic silica production and a disappearance of radiolarians, caused by an assumed rapid warming during the last Permian. Temperature changes as well as redox and alkalinity changes together with nutrient deficiency were considered as possible causes for the reduction of carbonate-stabilising benthic/nektonic and silicic silica-stabilising plankton (Isozaki et al. 2007). The occurrence of the pelagic community terminates 0.05 m below the extinction horizon; only ostracod valves and a mass occurrence of small ammonoids are recorded here.

The degree of bioturbation varies constantly between sparse and moderate in the upper part of the Hambast Formation (Fig. 11) with decreasing bioturbation and biogenic content immediately below the extinction horizon. Burrows are usually isolated and overlaps are rare. Using the index by Droser and Bottjer (1986), 10–40% of the sediment is affected by bioturbation. As the investigated succession of the Hambast Formation is characterised by rich benthic and pelagic assemblages and frequent bioturbation, we suggests a well-oxygenated environment for this interval.

Baghuk Member

The facies of the approximately two metres thick event interval represent the deposition conditions immediately after the main extinction pulse. In general, the Baghuk Member is separated from the carbonate-dominated Hambast-Formation by a sharp lithological contact caused by interrupted carbonate production. Limestone beds occur only occasionally in the Baghuk Member (Fig. 5). This facies was likely deposited in a low-energy environment with calm water conditions below the storm wave base (Mohtat Aghai et al. 2009; Leda et al. 2014).

Section C contains ‘calcite fans’ embedded in a matrix full of sponge spicules (at + 0.55 m and + 0.75 m). Time-equivalent structures are known from the Hambast sections and were first named ‘colonial limestones’ by Taraz

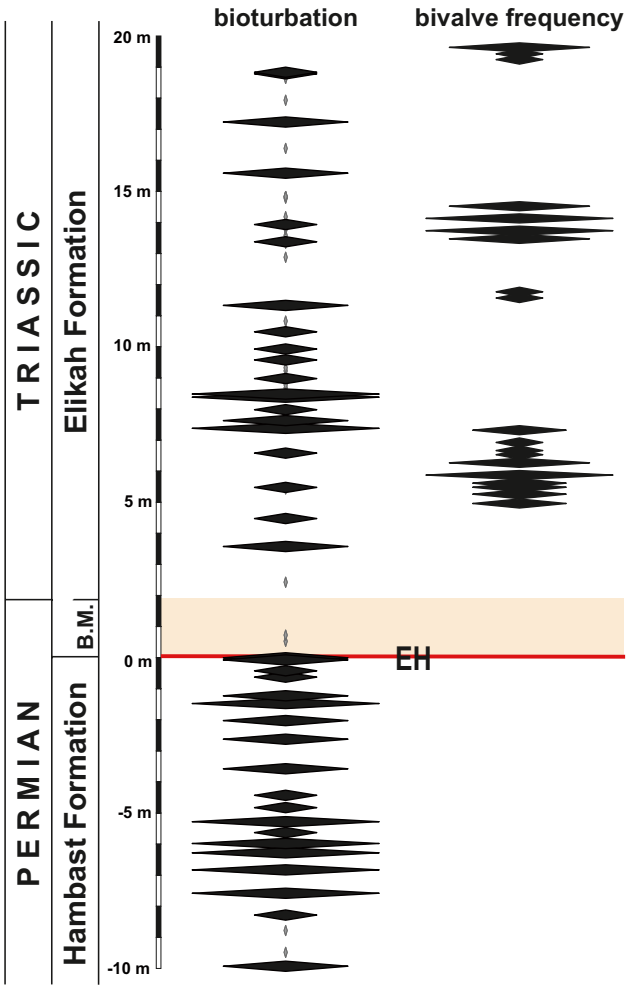

Fig. 11 Semi-quantitative frequency of bioturbation and large bivalves (*Claraia*, *Pseudomonotis*) across the Permian–Triassic boundary in Baghuk Mountain Sect. 1 (Hambast Formation) and section C (Elikah Formation). B.M. = Baghuk Member

et al. (1981) and later named'calcite fans ' by Heydari et al. (2003). Very similar calcite precipitates were already described, apart from sections in Central Iran, from Turkey and Armenia (Baud et al. 2007; Kershaw et al. 2012; Heindel et al. 2015; Friesenbichler 2016; Friesenbichler et al. 2018). Kershaw et al. (2012) interpreted such 'calcite fans' in the Hambast Range as crystal fans that grew on thinly laminated stromatolites. Recently, Baud et al. (2021) interpreted them as digitate stromatolites.

The 'calcite fan' formation was interpreted to have been caused by the dissolution of Ca^{2+} and HCO_3^- in seawater, which led to carbonate precipitation or degassing of CO_2 and consequently to a decrease in oceanic carbonate solubility (Woods et al. 1999, 2007; Heydari et al. 2003; Pruss and Bottjer 2004; Pruss et al. 2006). Woods et al. (1999) proposed a model in which a mixture of deep, anoxic, highly alkaline water and surface water favours the formation of seafloor cements and that this mixing leads to CO_2 degassing and carbonate supersaturation with $CaCO_3$.

The study by Friesenbichler (2016) of sections in Armenia dealt with the growth conditions of similar 'calcite fans' and their relationship to the surrounding sediment, as well as with the relationship between the occurrence of 'calcite fans' and sponges. She interpreted the asymmetric growth of the 'calcite fans' as being caused by steady bottom currents; this led to the assumption that they were formed on the sediment and not in the sediment (Friesenbichler 2016; Friesenbichler et al. 2018). In contrast, Heindel et al. (2015) preferred the displacement growth of crystals, which pushed away the surrounding sediment. This type of growth was neither found in the Armenian sections studied by Friesenbichler (2016) nor at Baghuk Mountain. Friesenbichler (2016) and Friesenbichler et al. (2018) assumed that 'calcite fans' grew before the sponge remains deposited. The sponge spicules fit to the crystal margins; they used the available space between the crystals and adapted their morphology.

Compared to the underlying Hambast-Formation, the biogenic content of the Baghuk Member is extremely low. Only in section C, few ammonoids, ostracods, echinoderms and bivalves were found at + 0.02 m, whereas sponges are conspicuously frequent. Bioturbation is also extremely sparse in the first few centimetres and disappears in the Baghuk Member.

Claraia Beds

The Early Triassic *Claraia* Beds begin above the Baghuk Member with a laminated wackestone that contains abundant calcite aggregates. This type of wackestone, which occurs at + 2.45 m and + 5.45 m (Fig. 8a), was already described by Richoz et al. (2010) from the Zal section and by Leda et al. (2014) from Ali Bashi in NW Iran. Both articles described them as seafloor cement crusts of sparse calcite spheres. The origin of these calcite spheres is still unknown; they are somewhat similar to those of tew same age found in deep water limestone from Oman (Baud et al. 2012). The moderately bioturbated mudstone above is characteristic for sedimentation conditions below the storm wave base. At + 8.00 m the first microbial structures appear as overgrowth on ammonoid and bivalve shells; presumably the shells were used as a hard substrate for the growth of the microbial structures. Microbialites occur in a number of beds (at + 7 to + 10 m, + 14 m and + 19.70 m) in Baghuk Mountain Section C (Fig. 5).

Early Triassic microbial deposits have been described from many regions and with varying morphological richness, but the environmental conditions for the growth of these structures are not yet fully understood. Various

hypotheses involving geochemical changes in seawater leading to carbonate factory alteration or atmospheric changes have already been postulated (e.g. Baud et al. 1997, 2007; Kershaw et al. 1999; Riding 2000; Kershaw et al. 2002, 2007, 2011, 2012; Ezaki et al. 2003, 2008; Pruss et al. 2006; Richoz et al. 2010; Yang et al. 2011; Tian et al. 2014; Zheng et al. 2016; Fang et al. 2017; Wu et al. 2017). Taraz et al. (1981) were the first to mention stromatolitic deposits in Early Triassic sections near Abadeh and interpreted them as thrombolites. These authors suggested a calm intertidal or subtidal depositional milieu for the stromatolite formation.

Apparently, all microbialites at Baghuk Mountain are accompanied by sponge spicules, which have been identified as keratose demosponges. Between the microbial horizons, wackestone to packstone with sponge spicules also occur without any microbial structure. This spiculite microfacies is typical of basal or deeper shelf environments (Flügel 2013, p. 682). Leda et al. (2014) described a sponge packstone in the Julfa sections (NW Iran) and postulated a deep carbonate shelf.

The biogenic content of the Early Triassic deposits immediately above the Baghuk Member is extremely low. The first occurrence of ostracods was recorded at + 3.60 m. Up to + 8.00 m only rare gastropods, ostracods and echinoderms occur, followed by mass occurrences of sponge spicules between + 9.00 m and + 10.00 m. In the Early Triassic interval from + 13.60 m to + 13.95 m sponges, foraminifers, ammonoids, ostracods, gastropods and echinoderms have their first co-occurrences.

The first sign of bioturbation is recorded at + 3.60 m (Fig. 11). Bioturbation occurs only in facies with microbial growth, whereas facies with individual micro-organisms do not contain bioturbation.

Discussion

Sea-level changes across the Permian–Triassic boundary

Heydari et al. (2003) postulated a significant sea-level drop at the end of the Permian for sections near Abadeh, followed by a rapid rise in the Early Triassic. The Early Triassic carbonates were there interpreted as shallow water deposits. Our microfacies analysis of the Baghuk Mountain sections show that the depositional environment of the entire section across the Permian–Triassic boundary shows no evidence of large-scale sea level changes or even subaerial exposure. With a few exceptions, the deposition probably took place on a deep shelf below the storm wave base. Richoz et al. (2010) and Leda et al. (2014) already identified such conditions in sections near Julfa (NW Iran). The Late Permian Hambast Formation including the *Paratirolites* Limestone equivalent at Baghuk Mountain is characterised by a typical deep shelf facies with benthic and pelagic assemblages. We agree with other authors that the Late Permian nodular facies were deposited in a deep shelf below the storm wave base (Heydari et al. 2000, 2003; Leda et al. 2014).

The marly facies of the Baghuk Member also does not show any indications for a sea-level drop, such as vadose meteoric cement types or palaeokarst. Sections in Julfa (NW-Iran) show a similar conditions without sedimentological evidence of large-scale sea-level changes at the Permian–Triassic boundary like other sections (Richoz et al. 2010).

Early Triassic microorganisms can provide an indication of shallowing after the extinction event. This coincides with the occurrence of large bivalves in chaotic position (mixed convex up and down) in some of the strata 8–9 m above the extinxtion horizon at Baghuk Mountain (Fig. 9d). These possible storm beds, which occur in immediate vicinity of microbiatites, may indicate episodic shallowing.

Carbonate production and ocean chemistry

At Baghuk Mountain, the biogen-dominated Permian carbonate factory was interrupted at the time of the end-Permian mass extinction, which is indicated by a sharp contact between the Hambast Formation and the Baghuk Member. The Baghuk Member is characterised by clay and/or silt deposits and few carbonate horizons. The synsedimentary carbonate precipitations were interpreted to be caused by a transition from biochemical to inorganic chemical carbonate production (Heydari et al. 2003). Heydari et al. (2008) postulated that a decrease in oceanic pH and an increase in seafloor carbonate saturation causes the change in carbonate production. This geochemical change is also supported by boron isotope records from sections in the Dolomites, indicating an acidification event at the extinction horizon (Jurikova et al. 2020). Furthermore, Heydari et al. (2008) recorded a mineralogical change from primary calcite in the Late Permian to aragonite after the mass extinction event and during the Early Triassic.

Conclusions

The investigation of the lithology and microfacies of the Permian–Triassic boundary section at Baghuk Mountain (Central Iran) led to the following results:

- In line with neighbouring sections near Shahreza and Abadeh, the sections of Baghuk Mountain consist of three lithostratigraphic units, in ascending order the Late Permian Hambast-Formation, the Baghuk Member of the latest Permian and the Early Triassic *Claraia* Beds. The latter two compose the Elikah Formation.
- The main Permian–Triassic extinction pulse has a position at the sharp lithological contact between the carbonate-dominated Hambast Formation and the shale and

marl-dominated Baghuk Member. It exactly coincides with the decease of the Late Permian carbonate factory.
- Changes in microfacies across the Permian–Triassic boundary in sections at Baghuk Mountain provide evidence for a change from Late Permian skeletal carbonate production to to a non-skeletal carbonate production in the Early Triassic.
- The upper ten metres of the Hambast Formation up to the Baghuk Member are strongly influenced by bioturbation, which suggests a well-oxygenated environment. The Baghuk Member shows no indications for bioturbation or relicts of benthic communities.
- In the Early Triassic, carbonate production was episodically induced by microbes and led to the formation of microbialites. The frequency of these microbial structures in the study area is remarkable.
- The carbonate deposition at Baghuk Mountain suggests a deep shelf environment, mostly below storm wave base. There is no evidence for a large scale sea-level change or subaerial exposure during the Permian–Triassic succession at Baghuk Mountain. During the Early Triassic, occasional shallowing led to tempestitic deposition of biogenes such as *Claraia* valves.

Acknowledgements We thank the Deutsche Forschungsgemeinschaft (DFG projects KO1829/12-1, KO1829/17-1, KO1829/18-1 and the TERSANE research unit FOR 2332) for financial support. Furthermore we would like to thank Sylvia Salzmann and Rudolf Knöfler (MfN Berlin) for the preparation of thin sections and polished rock samples. Axel Munnecke (University of Erlangen) is acknowledged for support with the microfacies analysis. For constructive comments we thank the reviewers Aymon Baud (Lausanne) and an anonymous reviewer.

Funding Open access funding provided by Museum für Naturkunde – Leibniz-Institut für Evolutions- und Biodiversitätsforschung (3498).

Declarations

Conflict of Interest The authors declare that they have no conflict of interest.

References

Aubouin, J. (1964). Reflexions sur le facies 'ammonitico rosso'. *Bulletin de la Société géologique de France*, *7*(4), 475–501.

Baccelle, L., & Bosellini, A. (1965). *Diagrammi per la stima visiva: della composizione percentuale nelle rocce sedimentarie*. Università degli studi di Ferrara.

Bando, Y. (1979). Upper Permian and Lower Triassic ammonoids from Abadeh, Central Iran. *Memoirs of the Faculty of Education, Kagawa University*, *23*, 103–138.

Bando, Y. (1981). Discovery of Lower Triassic ammonites in the Abadeh region of Central Iran. *Geological Survey of Iran, Report*, *49*, 73–103.

Baud, A. (2008). Correlation of Upper Permian localities in the Kuh-e-Ali Bashi area, NW Iran: old collections, old and new data. *Permophiles*, *52*, 6–11.

Baud, A., & Richoz, S. (2019). The latest Permian Red Ammonoid Limestone and the basal Triassic Sponge-Microbial buildups, Time Specific Facies on the Cimmerian margin of Central Iran and Armenia. *Società Geologica Italiana STRATI 2019*. p. 398.

Baud, A., Magaritz, M., & Holser, W. T. (1989). Permian-Triassic of the Tethys: Carbon isotope studies. *Geologische Rundschau*, *78*(2), 649–677.

Baud, A., Cirilli, S., & Marcoux, J. (1997). Biotic response to mass extinction: the lowermost Triassic microbialites. *Facies*, *36*, 238–242.

Baud, A., Richoz, S., & Pruss, S. (2007). The lower Triassic anachronistic carbonate facies in space and time. *Global and Planetary Change*, *55*(1), 81–89.

Baud, A., Richoz, S., Beauchamp, B., Cordey, F., Grasby, S., Henderson, C. M., Krystyn, L., & Nicora, A. (2012). The Buday'ah Formation, Sultanate of Oman: A Middle Permian to Early Triassic oceanic record of the Neotethys and the late Induan microsphere bloom. *Journal of Asian Earth Sciences*, *43*(1), 130–144.

Baud, A., Richoz, S., Brandner, R., Krystyn, L., Heindel, K., Mohtat, T., & Mohtat-Aghai, P. (2021). Sponge takeover from End-Permian mass extinction to early Induan time: Records in Central Iran microbial buildups. *Frontiers in Earth Science*, *8*, 586210.

Beauchamp, B., & Baud, A. (2002). Growth and demise of Permian biogenic chert along northwest Pangea: evidence for end-Permian collapse of thermohaline circulation. *Palaeogeography, Palaeoclimatology, Palaeoecology*, *184*(1-2), 37–63.

Berner, R. A. (2006). Carbon, sulfur and O2 across the Permian–Triassic boundary. *Journal of Geochemical Exploration*, *88*(1-3), 416–418.

Besse, J., Torcq, F., Gallet, Y., Ricou, L., Krystyn, L., & Saidi, A. (1998). Late Permian to Late Triassic palaeomagnetic data from Iran: constraints on the migration of the Iranian block through the Tethyan Ocean and initial destruction of Pangaea. *Geophysical Journal International*, *135*(1), 77–92.

Bond, D. P., & Wignall, P. B. (2010). Pyrite framboid study of marine Permian–Triassic boundary sections: a complex anoxic event and its relationship to contemporaneous mass extinction. *Geological Society of America Bulletin*, *122*(7-8), 1265–1279.

Burchette, T., & Wright, V. (1992). Carbonate ramp depositional systems. *Sedimentary Geology*, *79*(1), 3–57.

Burne, R. V., & Moore, L. S. (1987). Microbialites: organosedimentary deposits of benthic microbial communities. *Palaios*, 241–254.

Cecca, F., Fourcade, E., & Azéma, J. (1992). The disappearance of the "Ammonitico Rosso". *Palaeogeography, Palaeoclimatology, Palaeoecology*, *99*(1-2), 55–70.

Chen, B., Joachimski, M. M., Shen, S., Lambert, L. L., Lai, X., Wang, X., Chen, J., & Yuan, D. (2013). Permian ice volume and palaeoclimate history: oxygen isotope proxies revisited. *Gondwana Research*, *24*(1), 77–89.

Chen, Z.-Q., Wang, Y., Kershaw, S., Luo, M., Yang, H., Zhao, L., Feng, Y., Chen, J., Yang, L., & Zhang, L. (2014). Early Triassic stromatolites in a siliciclastic nearshore setting in northern Perth Basin, Western Australia: geobiologic features and implications

for post-extinction microbial proliferation. *Global and Planetary Change*, *121*, 89–100.

Chen, J., Shen, S., Zhang, Y., Angiolini, L., Gorgij, M. N., Crippa, G., Wang, W., Zhang, H., Yuan, D., & Li, X. (2020). Abrupt warming in the latest Permian detected using high-resolution in situ oxygen isotopes of conodont apatite from Abadeh, central Iran. *Palaeogeography, Palaeoclimatology, Palaeoecology*, 109973.

Droser, M. L., & Bottjer, D. J. (1986). A semiquantitative field classification of ichnofabric. *Journal of Sedimentary Research*, *56*(4).

Erwin, D. H. (1993). *The great Paleozoic crisis: life and death in the Permian*. New York: Columbia University Press.

Erwin, D. H. (1994). The Permo-Triassic extinction. *Nature*, *367*, 231–236.

Erwin, D. H., Bowring, S. A., & Jin, Y. (2002). End-Permian mass extinctions: a review. *Geological Society of America, Special Papers*, *356*, 363–384.

Ezaki, Y., Liu, J., & Adachi, N. (2003). Earliest Triassic microbialite micro- to megastructures in the Huaying area of Sichuan Province, South China: implications for the nature of oceanic conditions after the end-Permian extinction. *Palaios*, *18*(4), 388–402.

Ezaki, Y., Liu, J., Nagano, T., & Adachi, N. (2008). Geobiological aspects of the earliest Triassic microbialites along the southern periphery of the tropical Yangtze Platform: initiation and cessation of a microbial regime. *Palaios*, *23*(6), 356–369.

Fang, Y., Chen, Z.-Q., Kershaw, S., Yang, H., & Luo, M. (2017). Permian–Triassic boundary microbialites at Zuodeng Section, Guangxi Province, South China: Geobiology and palaeoceanographic implications. *Global and Planetary Change*, *152*, 115–128.

Farshid, E., Hamdi, B., Hairapetian, V., & Aghanabati, S. A. (2016). Conodont biostratigraphy of the Permian-Triassic boundary in the Baghuk mountain section Northwest of Abadeh. *Scientific Quarterly Journal, Geosciences*, *25*, 285–-294.

Flügel, E. (2013). *Microfacies of carbonate rocks. Analysis, interpretation and application. 2nd Edition*. Berlin, Heidelberg: Springer Science & Business Media.

Forel, M. B., Crasquin, S., Kershaw, S., & Collin, P. Y. (2013). In the aftermath of the end-Permian extinction: the microbialite refuge? *Terra Nova*, *25*(2), 137–143.

Foster, W. J., Heindel, K., Richoz, S., Gliwa, J., Lehrmann, D. J., Baud, A., Kolar-Jurkovšek, T., Aljinović, D., Jurkovšek, B., & Korn, D. (2020). Suppressed competitive exclusion enabled the proliferation of Permian/Triassic boundary microbialites. *The Depositional Record*, *6*(1), 62–74.

Friesenbichler, E., Richoz, S., Baud, A., Krystyn, L., Sahakyan, L., Vardanyan, S., Peckmann, J., Reitner, J., & Heindel, K. (2018). Sponge-microbial build-ups from the lowermost Triassic Chanakhchi section in southern Armenia: Microfacies and stable carbon isotopes. *Palaeogeography, Palaeoclimatology, Palaeoecology*, *490*, 653–672.

Friesenbichler, E. (2016) Sedimentological Investigations on Lower Triassic Microbialites from Armenia. Graz University of Technology

Gallet, Y., Krystyn, L., Besse, J., Saidi, A., & Ricou, L. E. (2000). New constraints on the Upper Permian and Lower Triassic geomagnetic polarity timescale from the Abadeh section (central Iran). *Journal of Geophysical Research: Solid Earth*, *105*(B2), 2805–2815.

Garrison, R. E., & Fischer, A. G. (1969). Deep-water limestones and radiolarites of the Alpine Jurassic. *SEPM Special Publication, 14*, 20–56.

Ghaderi, A., Leda, L., Schobben, M., Korn, D., & Ashouri, A. R. (2014). High-resolution stratigraphy of the Changhsingian (Late Permian) successions of NW Iran and the Transcaucasus based on lithological features, conodonts, and ammonoids. *Fossil Record*, *15*(1), 41–57.

Ghaedi, M., Mousavi, N., & Yazdi, M. (2009). Scrutiny and biozonation of Permian – Triassic boundary in Benarizeh area, north of Abadeh. (Paper presented at the Second conference of the Iranian Paleontological Association)

Gliwa, J., Ghaderi, A., Leda, L., Schobben, M., Tomás, S., Foster, W. J., Forel, M.-B., Ghanizadeh Tabrizi, N., Grasby, S. E., Struck, U., Ashouri, A. R., & Korn, D. (2020). Aras Valley (northwest Iran): high-resolution stratigraphy of a continuous central Tethyan Permian–Triassic boundary section. *Fossil Record*, *23*(1), 33-69.

Hallam, A., & Wignall, P. (1999). Mass extinctions and sea-level changes. *Earth-Science Reviews*, *48*(4), 217–250.

Hampe, O., Hairapetian, V., Dorka, M., Witzmann, F., Akbari, A. M., & Korn, D. (2013). A first late Permian fish fauna from Baghuk Mountain (Neo-Tethyan shelf, central Iran). *Bulletin of Geosciences*, *88*(1), 1-20.

Heindel, K., Richoz, S., Birgel, D., Brandner, R., Klügel, A., Krystyn, L., Baud, A., Horacek, M., Mohtat, T., & Peckmann, J. (2015). Biogeochemical formation of calyx-shaped carbonate crystal fans in the subsurface of the Early Triassic seafloor. *Gondwana Research*, *27*(2), 840–861.

Heydari, E., & Hassanzadeh, J. (2003). Deev Jahi model of the Permian–Triassic boundary mass extinction: a case for gas hydrates as the main cause of biological crisis on Earth. *Sedimentary Geology*, *163*(1), 147–163.

Heydari, E., Hassandzadeh, J., & Wade, W. (2000). Geochemistry of central Tethyan upper Permian and lower Triassic strata, Abadeh region, Iran. *Sedimentary Geology*, *137*(1), 85–99.

Heydari, E., Wade, W. J., & Hassanzadeh, J. (2001). TethyanDiagenetic origin of carbon and oxygen isotope compositions of Permian–Triassic boundary strata. *Sedimentary Geology*, *143*(3), 191–197.

Heydari, E., Hassanzadeh, J., Wade, W., & Ghazi, A. (2003). Permian–Triassic boundary interval in the Abadeh section of Iran with implications for mass extinction: Part 1–Sedimentology. *Palaeogeography, Palaeoclimatology, Palaeoecology*, *193*(3), 405–423.

Heydari, E., Arzani, N., & Hassanzadeh, J. (2008). Mantle plume: the invisible serial killer—application to the Permian–Triassic boundary mass extinction. *Palaeogeography, Palaeoclimatology, Palaeoecology*, *264*(1), 147–162.

Heydari, E., Arzani, N., Safaei, M., & Hassanzadeh, J. (2013). Ocean's response to a changing climate: Clues from variations in carbonate mineralogy across the Permian–Triassic boundary of the Shareza Section, Iran. *Global and Planetary Change*, *105*, 79–90.

Horacek, M., Richoz, S., Brandner, R., Krystyn, L., & Spötl, C. (2007a). Evidence for recurrent changes in Lower Triassic oceanic circulation of the Tethys: the δ13C record from marine sections in Iran. *Palaeogeography, Palaeoclimatology, Palaeoecology*, *252*(1), 355–369.

Horacek, M., Richoz, S., Brandner, R., Krystyn, L., & Spötl, C. (2007b). Evidence for recurrent changes in Lower Triassic oceanic circulation of the Tethys: the δ 13 C record from marine sections in Iran. *Palaeogeography, Palaeoclimatology, Palaeoecology*, *252*(1), 355–369.

Horacek, M., Krystyn, L., & Baud, A. (2021). Comment to Chen et al., 2020: "Abrupt warming in the latest Permian detected using high-resolution in situ oxygen isotopes of conodont apatite from Abadeh, central Iran." Importance of correct stratigraphic correlation, reporting of existing data and their scientific interpretation. *Permophiles*, *70*, 33–36.

Isozaki, Y., Shimizu, N., Yao, J., Ji, Z., & Matsuda, T. (2007). End-Permian extinction and volcanism-induced environmental stress: the Permian–Triassic boundary interval of lower-slope facies at Chaotian, South China. *Palaeogeography, Palaeoclimatology, Palaeoecology*, *252*(1-2), 218–238.

Jenkyns, H. C. (1991). Origin of red nodular limestones (Ammonitico Rosso, Knollenkalke) in the Mediterranean Jurassic: a diagenetic model. In K. J. Hsü, & H. C. Jenkyns (Eds.) *Pelagic Sediments: On Land and Under the Sea*. *IAS Special Publications*, *1*, 249–271.

Joachimski, M. M., Lai, X., Shen, S., Jiang, H., Luo, G., Chen, B., Chen, J., & Sun, Y. (2012). Climate warming in the latest Permian and the Permian–Triassic mass extinction. *Geology*, *40*(3), 195–198.

Joachimski, M. M., Alekseev, A. S., Grigoryan, A., & Gatovsky, Y. A. (2020). Siberian Trap volcanism, global warming and the Permian-Triassic mass extinction: New insights from Armenian Permian-Triassic sections. *GSA Bulletin*, *132*(1-2), 427–443.

Jurikova, H., Gutjahr, M., Wallmann, K., Flögel, S., Liebetrau, V., Posenato, R., Angiolini, L., Garbelli, C., Brand, U., & Wiedenbeck, M. (2020). Permian–Triassic mass extinction pulses driven by major marine carbon cycle perturbations. *Nature Geoscience*, *13*(11), 745–750.

Kershaw, S., Zhang, T., & Lan, G. (1999). A ?microbialite carbonate crust at the Permian–Triassic boundary in South China, and its palaeoenvironmental significance. *Palaeogeography, Palaeoclimatology, Palaeoecology*, *146*(1), 1–18.

Kershaw, S., Guo, L., Swift, A., & Fan, J. (2002). ?Microbialites in the Permian-Triassic boundary interval in central China: Structure, age and distribution. *Facies*, *47*(1), 83–89.

Kershaw, S., Li, Y., Crasquin-Soleau, S., Feng, Q., Mu, X., Collin, P.-Y., Reynolds, A., & Guo, L. (2007). Earliest Triassic microbialites in the South China block and other areas: controls on their growth and distribution. *Facies*, *53*(3), 409–425.

Kershaw, S., Crasquin, S., Forel, M.-B., Randon, C., Collin, P.-Y., Kosun, E., Richoz, S., & Baud, A. (2011). Earliest Triassic microbialites in Çürük Dag, southern Turkey: composition, sequences and controls on formation. *Sedimentology*, *58*(3), 739–755.

Kershaw, S., Crasquin, S., Li, Y., Collin, P.-Y., Forel, M.-B., Mu, X., Baud, A., Wang, Y., Xie, S., & Maurer, F. (2012). Microbialites and global environmental change across the Permian–Triassic boundary: a synthesis. *Geobiology*, *10*(1), 25–47.

Knoll, A. H., Bambach, R. K., Canfield, D. E., & Grotzinger, J. P. (1996). Comparative earth history and late permian mass extinction. *Science*, *273*(5274), 452–457.

Korn, D., Ghaderi, A., & Ghanizadeh Tabrizi, N. (2019). Early Changhsingian (Late Permian) ammonoids from NW Iran. *Neues Jahrbuch für Geologie und Paläontologie-Abhandlungen*, *293*(1), 37–56.

Korn, D., Leda, L., Heuer, F., Moradi Salimi, H., Farshid, E., Akbari, A., Schobben, M., Ghaderi, A., Struck, U., Gliwa, J., Ware, D., & Hairapetian, V. (2021). Baghuk Mountain (Central Iran): high-resolution stratigraphy of a continuous Central Tethyan Permian–Triassic boundary section. *Fossil Record*, *24*, 171–192.

Korte, C., Kozur, H. W., Joachimski, M. M., Strauss, H., Veizer, J., & Schwark, L. (2004a). Carbon, sulfur, oxygen and strontium isotope records, organic geochemistry and biostratigraphy across the Permian/Triassic boundary in Abadeh, Iran. *International Journal of Earth Sciences*, *93*(4), 565–581.

Korte, C., Kozur, H. W., & Mohtat-Aghai, P. (2004b). Dzhulfian to lowerest Triassic delta 13 C record at the Permian/Triassic boundary section at Shahreza, Central Iran. *Hallesches Jahrbuch für Geowissenschaften, Reihe B, Beiheft*, *18*, 73–78.

Korte, C., Pande, P., Kalia, P., Kozur, H. W., Joachimski, M. M., & Oberhänsli, H. (2010). Massive volcanism at the Permian–Triassic boundary and its impact on the isotopic composition of the ocean and atmosphere. *Journal of Asian Earth Sciences*, *37*(4), 293–311.

Kozur, H. W. (2004). Pelagic uppermost Permian and the Permian-Triassic boundary conodonts of Iran. Part I: taxonomy. *Hallesches Jahrbuch für Geowissenschaften, Reihe B, Beiheft*, *18*, 39–68.

Kozur, H. W. (2005). Pelagic uppermost Permian and the Permian-Triassic boundary conodonts of Iran. Part II: Investigated sections and evaluation of the conodont faunas. *Hallesches Jahrbuch für Geowissenschaften, Reihe B, Beiheft*, *19*, 49–86.

Kozur, H. W. (2007). Biostratigraphy and event stratigraphy in Iran around the Permian–Triassic Boundary (PTB): implications for the causes of the PTB biotic crisis. *Global and Planetary Change*, *55*(1), 155–176.

Leda, L., Korn, D., Ghaderi, A., Hairapetian, V., Struck, U., & Reimold, W. U. (2014). Lithostratigraphy and carbonate microfacies across the Permian–Triassic boundary near Julfa (NW Iran) and in the Baghuk Mountains (Central Iran). *Facies*, *60*(1), 295–325.

Leda, L. (2020) The Permian-Triassic boundary in the NW-Iranian Transcaucasus and in Central Iran. Doctoral Thesis, Humboldt-Universität zu Berlin, 222 pp. https://doi.org/10.18452/21106

Liu, X., Wang, W., Shen, S., Gorgij, M. N., Ye, F., Zhang, Y., Furuyama, S., Kano, A., & Chen, X. (2013). Late Guadalupian to Lopingian (Permian) carbon and strontium isotopic chemostratigraphy in the Abadeh section, central Iran. *Gondwana Research*, *24*(1), 222–232.

Mamet, B., & Préat, A. (2006). Iron-bacterial mediation in Phanerozoic red limestones: state of the art. *Sedimentary Geology*, *185*(3), 147–157.

Mata, S., & Bottjer, D. (2012). Microbes and mass extinctions: paleoenvironmental distribution of microbialites during times of biotic crisis. *Geobiology*, *10*(1), 3–24.

Mohtat Aghai, P., Vachard, D., & Krainer, K. (2009). Transported foraminifera in Palaeozoic deep red nodular limestones exemplified by latest Permian Neoendothyra in the Zal section (Julfa area, NW Irán. *Revista Española de Micropaleontología*, *41*(1-2), 197–213.

Mohtat-Aghai, P., & Vachard, D. (2005). Late Permian foraminiferal assemblages from the Hambast region (central Iran) and their extinctions. *Revista Española de Micropaleontología*, *37*, 205–227.

Nabavi, M. H. (1976). An introduction to the geology of Iran. *Geological Survey of Iran Publications*, *109*.

Noble, J., & Howells, K. (1974). Early marine lithification of the nodular limestones in the Silurian of New Brunswick. *Sedimentology*, *21*(4), 597–609.

Partoazar, H. (2002). Permian-Triassic boundary conodonts from Jolfa-Abadeh Belt along Northwest and Central Iran. *Permophiles*, *41*, 34–40.

Pruss, S. B., & Bottjer, D. J. (2004). Late Early Triassic microbial reefs of the western United States: a description and model for their deposition in the aftermath of the end-Permian mass extinction. *Palaeogeography, Palaeoclimatology, Palaeoecology*, *211*(1), 127–137.

Pruss, S. B., Bottjer, D. J., Corsetti, F. A., & Baud, A. (2006). A global marine sedimentary response to the end-Permian mass extinction: examples from southern Turkey and the western United States. *Earth-Science Reviews*, *78*(3), 193–206.

Raup, D. M., & Sepkoski, J. J. (1982). Mass extinctions in the marine fossil record. *Science*, *215*(4539), 1501–1503.

Raup, D. M., & Sepkoski, J. J. (1984). Periodicity of extinctions in the geologic past. *Proceedings of the National Academy of Sciences*, *81*(3), 801–805.

Reineck, H.-E. (1967). Parameter von Schichtung und Bioturbation. *Geologische Rundschau*, *56*(1), 420–438.

Richoz, S., Krystyn, L., Baud, A., Brandner, R., Horacek, M., & Mohtat-Aghai, P. (2010). Permian–Triassic boundary interval in the Middle East (Iran and N. Oman): Progressive environmental change from detailed carbonate carbon isotope marine curve and sedimentary

evolution. *Journal of Asian Earth Sciences*, *39*(4), 236–253. http://dx.doi.org/https://doi.org/10.1016/j.jseaes.2009.12.014.

Riding, R. (2000). Microbial carbonates: the geological record of calcified bacterial–algal mats and biofilms. *Sedimentology*, *47*(s1), 179–214.

Ruban, D. A., Al-Husseini, M. I., & Iwasaki, Y. (2007). Review of Middle east Paleozoic plate tectonics. *GeoArabia*, *12*(3), 35–56.

Schlager, W. (2002). *Sedimentology and sequence stratigraphy of carbonate rocks*. Amsterdam: Frije Universiteit, Amsterdam.

Schobben, M., Joachimski, M. M., Korn, D., Leda, L., & Korte, C. (2014). Palaeotethys seawater temperature rise and an intensified hydrological cycle following the end-Permian mass extinction. *Gondwana Research*, *26*, 675–683.

Schobben, M., Stebbins, A., Ghaderi, A., Strauss, H., Korn, D., & Korte, C. (2015). Flourishing ocean drives the end-Permian marine mass extinction. *Proceedings of the National Academy of Sciences*, *112*(33), 10298–10303.

Schobben, M., Foster, W. J., Sleveland, A. R., Zuchuat, V., Svensen, H. H., Planke, S., Bond, D. P., Marcelis, F., Newton, R. J., & Wignall, P. B. (2020). A nutrient control on marine anoxia during the end-Permian mass extinction. *Nature Geoscience*, *13*, 640–646.

Schobben, M., Stebbins, A., Algeo, T. J., Strauss, H., Leda, L., Haas, J., Struck, U., Korn, D., & Korte, C. (2017). Volatile earliest Triassic sulfur cycle: A consequence of persistent low seawater sulfate concentrations and a high sulfur cycle turnover rate? *Palaeogeography, Palaeoclimatology, Palaeoecology*, *486*, 74–85.

Shapiro, R. S. (2000). A comment on the systematic confusion of thrombolites. *Palaios, 15*(2), 166–169.

Stampfli, G. M., & Borel, G. D. (2004). The TRANSMED transects in space and time: constraints on the paleotectonic evolution of the Mediterranean domain. *The TRANSMED Atlas. The Mediterranean region from crust to mantle* (pp. 53–80). Springer.

Stampfli, G. M., & Borel, G. (2002). A plate tectonic model for the Paleozoic and Mesozoic constrained by dynamic plate boundaries and restored synthetic oceanic isochrons. *Earth and Planetary Science Letters*, *196*(1), 17–33.

Stanley, S. M., & Yang, X. (1994). A double mass extinction at the end of the paleozoic era. *Science*, *266*(5189), 1340–1344. http://www.sciencemag.org/content/266/5189/1340.abstract.

Stepanov, D. L., Golshani, F., & Stöcklin, J. (1969). Upper Permian and Permian-Triassic boundary in North Iran. *Geolological Survey of Iran, Report*, *12*, 1–72.

Stöcklin, J. (1968). Structural history and tectonics of Iran: a review. *AAPG Bulletin*, *52*(7), 1229–1258.

Sun, Y., Joachimski, M. M., Wignall, P. B., Yan, C., Chen, Y., Jiang, H., Wang, L., & Lai, X. (2012). Lethally hot temperatures during the Early Triassic greenhouse. *Science*, *338*(6105), 366–370.

Taraz, H. (1969). Permo-Triassic section in central Iran. *AAPG Bulletin*, *53*(3), 688–693.

Taraz, H. (1971). Uppermost Permian and Permo-Triassic transition beds in central Iran. *AAPG Bulletin*, *55*(8), 1280–1294.

Taraz, H. (1974). Geology of the Surmaq Deh Bid Area, Abadeh Region, Central Iran. *Geological Survey of Iran, Reports*, *37*(37), 1–148.

Taraz, H. (1973). Correlation of uppermost Permian in Iran, central Asia, and south China. *AAPG Bulletin, 57*(6), 1117–1133.

Taraz, H., Golshani, F., Nakazawa, K., Sgimuzu, D., Bando, Y., Ishi, K., Murata, M., Okimura, Y., Sakagami, S., Nakamura, K., & Tokuoka, T. (1981). The Permian and the Lower Triassic Systems in Abadeh Region, Central Iran. *Memoirs of the Faculty of Science, Kyoto University, Series of Geology and Mineralogy*, *47*(2), 61–133.

Taylor, A., & Goldring, R. (1993). Description and analysis of bioturbation and ichnofabric. *Journal of the Geological Society*, *150*(1), 141-148.

Teichert, C., Kummel, B., & Sweet, W. C. (1973). Permian-Triassic strata, Kuh-e-Ali Bashi, Northwestern Iran. *Bulletin of the Museum of Comparative Zoology, Harvard University*, *145*(8), 359–472.

Tian, L., Tong, J., Sun, D., Xiong, Y., Wang, C., Song, H., Song, H., & Huang, Y. (2014). The microfacies and sedimentary responses to the mass extinction during the Permian-Triassic transition at Yangou Section, Jiangxi Province, South China. *Science China Earth Sciences*, *57*(9), 2195-2207.

Torsvik, T. H., & Cocks, L. R. M. (2004). Earth geography from 400 to 250 Ma: a palaeomagnetic, faunal and facies review. *Journal of the Geological Society*, *161*(4), 555-572.

Tucker, M. E. (1974). Sedimentology of Palaeozoic pelagic limestones: the Devonian Griotte (Southern France) and Cephalopodenkalk (Germany). In K. J. Hsu, and H. C. Jenkyns (Eds.), *Pelagic sediments: on Land and under the Sea* (pp. 71-92). Oxford, London, Edinburgh, Melbourne: Blackwell Scientific Publications.

Wendt, J., & Aigner, T. (1985). Facies patterns and depositional environments of Palaeozoic cephalopod limestones. *Sedimentary Geology*, *44*(3-4), 263-300.

Wignall, P. B., & Hallam, A. (1992). Anoxia as a cause of the Permian/Triassic mass extinction: facies evidence from northern Italy and the western United States. *Palaeogeography, Palaeoclimatology, Palaeoecology*, *93*(1-2), 21-46.

Wignall, P. B., & Twitchett, R. J. (1996). Oceanic anoxia and the end Permian mass extinction. *Science*, *272*(5265), 1155-1158.

Wilson, J. L. (1975). *Carbonate facies in geologic history*. New York: Springer.

Woods, A. D., Bottjer, D. J., Mutti, M., & Morrison, J. (1999). Lower Triassic large sea-floor carbonate cements: Their origin and a mechanism for the prolonged biotic recovery from the end-Permian mass extinction. *Geology*, *27*(7), 645-648.

Woods, A. D., Bottjer, D. J., & Corsetti, F. A. (2007). Calcium carbonate seafloor precipitates from the outer shelf to slope facies of the Lower Triassic (Smithian-Spathian) Union Wash Formation, California, USA: Sedimentology and palaeobiologic significance. *Palaeogeography, Palaeoclimatology, Palaeoecology*, *252*(1), 281-290.

Wu, S., Chen, Z., Fang, Y., Pei, Y., Yang, H., & Ogg, J. (2017). A Permian-Triassic boundary microbialite deposit from the eastern Yangtze Platform (Jiangxi Province, South China): Geobiologic features, ecosystem composition and redox conditions. *Palaeogeography, Palaeoclimatology, Palaeoecology*, *486*, 58-73.

Yang, H., Chen, Z., Wang, Y., Tong, J., Song, H., & Chen, J. (2011). Composition and structure of microbialite ecosystems following the end-Permian mass extinction in South China. *Palaeogeography, Palaeoclimatology, Palaeoecology*, *308*(1), 111-128.

Zakharov, Y. D., Abnavi, N. M., Yazdi, M., & Ghaedi, M. (2010). New species of Dzhulfian (Late Permian) ammonoids from the Hambast Formation of Central Iran. *Paleontological Journal*, *44*(6), 614-621.

Zhang, F., Romaniello, S. J., Algeo, T. J., Lau, K. V., Clapham, M. E., Richoz, S., Herrmann, A. D., Smith, H., Horacek, M., & Anbar, A. D. (2018). Multiple episodes of extensive marine anoxia linked to global warming and continental weathering following the latest Permian mass extinction. *Science advances*, *4*(4), e1602921.

Zheng, Q., Cao, C., Wang, Y., Zhang, H., & Ding, Y. (2016). Microbialite concretions in a dolostone crust at the Permian–Triassic boundary of the Xishan section in Jiangsu Province, South China. *Palaeoworld*, *25*(2), 188-198.Baghuk Mountain after Farshid